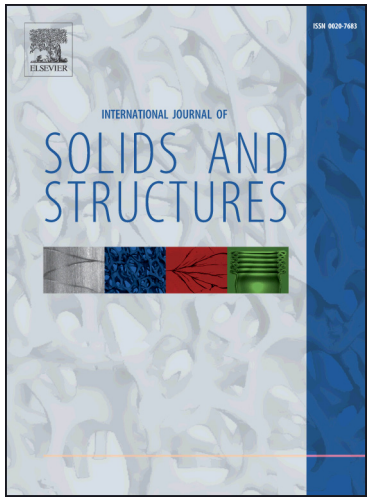
Accepted Manuscript



An extended semi-analytical formulation for fast and reliable mode I/II stress analysis of adhesively bonded joints

G. Lelias, E. Paroissien, F. Lachaud, J. Morlier, S. Schwartz, C. Gavoille

PII: S0020-7683(14)00497-1
DOI: http://dx.doi.org/10.1016/j.ijsolstr.2014.12.027
Reference: SAS 8608

To appear in: *International Journal of Solids and Structures*

Received Date: 17 September 2014
Revised Date: 23 December 2014

Please cite this article as: Lelias, G., Paroissien, E., Lachaud, F., Morlier, J., Schwartz, S., Gavoille, C., An extended semi-analytical formulation for fast and reliable mode I/II stress analysis of adhesively bonded joints, *International Journal of Solids and Structures* (2015), doi: http://dx.doi.org/10.1016/j.ijsolstr.2014.12.027

This is a PDF file of an unedited manuscript that has been accepted for publication. As a service to our customers we are providing this early version of the manuscript. The manuscript will undergo copyediting, typesetting, and review of the resulting proof before it is published in its final form. Please note that during the production process errors may be discovered which could affect the content, and all legal disclaimers that apply to the journal pertain.

ACCEPTED MANUSCRIPT

An extended semi-analytical formulation for fast and reliable mode I/II stress analysis of adhesively bonded joints

G. LELIAS[1,2,*], E. PAROISSIEN[1], F. LACHAUD[2], J. MORLIER[2], S. SCHWARTZ[1] and C. GAVOILLE[1]

[1]*SOGETI HIGH TECH, Parc le Millénaire - Bât A1, Avenue de l'Escadrille Normandie Niemen, 31700 BLAGNAC, FRANCE*

[2]*Université de Toulouse, Institut Clément Ader, ISAE, 10 Avenue Edouard Belin, 31055 TOULOUSE Cedex 4, FRANCE*

Running Head: An extended semi-analytical formulation for fast and reliable mode I/II stress analysis of adhesively bonded joints

*To whom correspondence should be addressed: Tel. +33534362684, Fax. +33534362626, E-mail: guillaume.lelias@sogeti.com

ACCEPTED MANUSCRIPT

ACCEPTED MANUSCRIPT

Abstract – The Finite Element (FE) method is able to address the stress analysis of adhesively bonded joints. However, analyses based on FE models are computationally expansive and it would be profitable to develop simplified approaches enabling extensive parametric studies. Firstly, a 1D-beam simplified model for the bonded joint stress analysis assuming a linear elastic adhesive material is presented. This model, derived from an approach inspired by the Finite Element (FE) method and based on the semi-analytical formulation of a 4-nodes macro-element, is able to simulate entire bonded overlaps at low computational costs. Secondly, a numerical procedure allowing for non-linear adhesive stress-strain relationships to be accounted for is presented. This procedure allows for various non-linear adhesive behaviors (ie. softening, plastic, etc.) to be accounted for with no restriction on the specimen geometry. The possible mixed-mode I/II response of the adhesive layer is introduced through an extension of the classical Cohesive Zone Modeling (CZM) procedure. The aforementioned procedure is then illustrated using a bi-linear softening adhesive behavior. However the procedure is not limited to this particular behavior only. The results obtained are finally compared to those of more time-consuming 2D FE strength predictions. Good agreement is shown.

keywords: *bonded joints, adhesive joints, semi-analytical resolution procedure, macro-element, cohesive zone modeling, mixed-mode I/II, Finite Element analyses*

NOMENCLATURES AND UNITS

A_j	extensional stiffness (N) of the adherend *j*
B_j	extensional and bending coupling stiffness (N.mm) of the adherend *j*
D_j	bending stiffness (N.mm^2) of the adherend *j*
e	thickness of the adhesive layer (mm)
E	Young's modulus (MPa) of the adhesive
E_j	Young's modulus (MPa) of the adherend *j*
$\boldsymbol{F}$	vector of nodal forces

ACCEPTED MANUSCRIPT

G	Coulomb's modulus (MPa) of the adhesive
$\boldsymbol{K}$	stiffness matrix
$\boldsymbol{K_{BBe}}$	stiffness matrix of the Bonded-Beam macro-element
L	length (mm) of the overlap
M_j	bending moment (N.mm) in the adherend j around the z direction
N_j	normal force (N) in the adherend j in the x direction
Q_σ	nodal normal force (N) applied to the node σ in the x direction ($\sigma = i,j,k,l$)
$\boldsymbol{R}$	vector of imbalanced loads (N)
R_σ	nodal shear force (N) applied to the node σ in the y direction ($\sigma = i,j,k,l$)
S	adhesive peel stress (MPa)
S_σ	nodal bending moment (N.mm) applied to the node σ around the z direction ($\sigma = i,j,k,l$)
T	adhesive shear stress (MPa)
$\boldsymbol{U}$	vector of nodal displacements
V_j	shear force (N) in the adherend j in the y direction
b	width (mm) of the adherends
e	thickness (mm) of the adhesive
e_j	thickness (mm) of the adherend j
n	number of macro-elements
u_j	displacement (mm) of the adherend j in the x direction
u_a	displacement (mm) of the node a in the x direction ($a = i,j,k,l$)
w_j	displacement (mm) of the adherend j in the y direction
w_a	displacement (mm) of the node a in the y direction ($a = i,j,k,l$)
Δ	length (mm) of a macro-element
η	characteristic constant
ρ	characteristic constant
ν_j	Poisson's ratio of the adherend j
θ_j	angular displacement (rad) of the adherend j around the z direction
θ_a	angular displacement (rad) of the node a around the z direction ($a = i,j,k,l$)

ACCEPTED MANUSCRIPT

ACCEPTED MANUSCRIPT

(x,y,z)	system of coordinates
Centrifugal forces	Forces that depend on the vector of nodal displacements (ie. load pressure, centrifugal forces, etc.).
Peel modulus	Since the traction properties of thin adhesive layers has been largely shown as different to those of bulk specimens, the peel modulus refers to the effective modulus of the adhesive layer when subjected to pure traction loads (see Appendix.2).
ENF	End Notched Flexure
DCB	Double Cantilever Beam
MMB	Mixed Mode Bending
bSLJ	balanced Single-Lap Joint
IbSLJ	imbalanced Single-Lap Joint
CLS	Cracked-Lap Shear
T-Stiff	T-Stiffener
V-Stiff	V-Stiffener
Normalized deviation	Normalized difference between semi-analytical results and Finite Elements predictions ($E = (X_{BBe}-X_{FE})/max(X_{FE})$)
DoF	Degrees of Freedom

1. INTRODUCTION

1.1. Context

In the frame of the design of structural components, the choice of joining technologies is essential. Adhesive bonding can be considered as an attractive joining technology, compared to conventional ones, such as bolting or riveting. Indeed, adhesive bonding offers the possibility of joining without damaging various combinations of materials, including plastics and metals. Moreover, since the amount of adhesive required to sustain static or fatigue loads is very low, adhesive bonding allows for weight benefits. However,

ACCEPTED MANUSCRIPT

ACCEPTED MANUSCRIPT

the interest of adhesive bonding remains while the integrity of the joint is ensured. To take advantage of adhesive bonding, accurate strength predictions are thus required.

The strength prediction of bonded joints requires the determination of computed criteria and experimentally characterized allowable. Several approaches are proposed in the open literature. These approaches could besides be used in the experimental characterization process of allowable.

The stress analysis approach, based on the Strength of Materials, is the classical approach. It aims at localizing the maximal values of stresses and strains, as highlighted in several literature surveys (Igen 1993, Tsai 1994, Da Silva 2009, Da Silva 2012). Another approach is based on the Fracture Mechanics. Assuming the presence of an initial crack, judiciously localized and sized by the user, it allows for the computation of strain energy release rate or J-integral parameters at crack tip as a function of applied forces or adhesive stresses (Fraise 1993, Tong 1994, Fernlund 2007, Da Silva 2012). In the coupled stress and energy criterion approach, the crack length at initiation is not assumed but derived from the analysis (Leguillon 2002, Weissgraeber 2013). Then, the computed crack length at initiation is not a material characteristic and depends both on geometrical parameters as well as on material critical stress and energy release rate. Finally, the Cohesive Zone Modeling – denoted CZM – is based on Damage Mechanics. It enables a diagnostic of the current damage state and an update of the strength prediction. The damage, associated to micro-cracks or voids, results in a progressive degradation of the material stiffness before failure. Both damage initiation and propagation phases are included in the formulation, without assuming any initial cracks (Valoroso 2004, De Moura 2008, Campilho 2013). Experimental approaches based on classical Fracture Mechanics tests allow for the characterization of the mechanical constitutive cohesive behavior of adhesive layers (Biel 2008, Anyfantis 2012).

1.2. Objective

ACCEPTED MANUSCRIPT

The Finite Element – denoted FE – method is able to address the stress, fracture and damage analyses of bonded joints (Da Silva 2009). Nevertheless, since analyses based on FE models are computationally expansive, it would be profitable both to restrict them to refined analyses and to develop for designers simplified approaches, enabling extensive parametric studies. The objective of this paper is then to present a simplified model for the mixed-mode I/II non-linear strength analysis of adhesively bonded joints.

A large number of simplified approaches for the stress analysis of bonded joints exist in the open literature (Igen 1993, Tsai 1994, Da Silva 2009). The joint kinematic is then simplified. The displacement field of adherends is supposed relevant to the beam or plate theory while the adhesive displacement field is expressed in terms of that of adherends (then restricting the number of components of the adhesive stress tensor). A direct limitation of this simplification is that out-of-plane deformations may not occur within the present model. A widespread modeling of the adhesive layer consists in an elastic foundation, supporting both adherends interfaces (Volkersen 1938, Goland & Reissner 1944, Hart-Smith 1973a, Hart-Smith 1973b). The adhesive stresses are then function of the relative displacements of the adherends interfaces, which is consistent with the CZM. Depending on the additional simplifying hypotheses taken, a closed-form solution is not always available, so that mathematical procedures (Mortensen 1998, Oterkus 2004, Paroissien *et al.* 2013) are needed to integrate the governing system of differential equations in view of boundary conditions.

The semi-analytical solution presented in (Paroissien *et al.* 2013) considers the adherends as Euler-Bernoulli laminated beams supported by an infinite number of elastic shear and peel springs. Besides, an original procedure allowing for non-linear adhesive behaviors to be accounted for is presented. However, the authors show that the aforementioned procedure is theoretically limited to the analysis of single-lap joint configurations and sufficiently small material nonlinearities only.

In the present paper, a reworked semi-analytical procedure enabling for various non-linear adhesive behaviors to be accounted for with no restriction on the specimen geometry is presented. The possible mixed mode I/II response of the adhesive layer is

ACCEPTED MANUSCRIPT

introduced through an extension of the classical CZM procedure (Valoroso 2004, De Moura 2008, Anyfantis 2012, Campilho 2013). The semi-analytical procedure is illustrated using a bi-linear softening, an exponential softening, a polynomial softening and a perfectly plastic adhesive stress-strain evolution law. The results obtained with the simplified 1D-beam model are then compared to those of 2D FE analyses.

1.3. Overview of the paper

In a first part, for lecturer comfort, a short description of the original linear elastic 1D-beam model for the stress analysis of a single-lap bonded joint is provided. A full description of the model can be found in (Paroissien *et al.* 2013). In a second part, an original procedure allowing for the mixed-mode I/II response of the adhesive layer to be addressed is presented. In a third part, an iterative procedure based on an adaptation of the classical Newton-Raphson iterative procedure, and allowing for various non-linear adhesive stress-strain relationships to be accounted for, is presented and developed in view of its implementation. Finally, the results obtained from the simplified 1D-beam model are compared with those of 2D FE models involving cohesive interface elements.

2. LINEAR ELASTIC 1D-BEAM MODEL

2.1. Overview

The simplified linear elastic method is inspired by the FE method and allows for the resolution of the bonded overlap system of governing differential equations. The displacements and forces of both adherends, as well as the adhesive stresses, are then computed. The method consists in meshing the structure. A fully bonded overlap is meshed using a unique 4-nodes macro-element, which is specially formulated to allow for the resolution of the bonded overlap system of governing differential equations. For convenience, this macro-element is thereafter referred as the Bonded-Beam (BBe)

ACCEPTED MANUSCRIPT

element. The outer adherends are meshed using classical Euler-Bernoulli beam elements. According to the classical FE rules, the stiffness matrix of the entire structure – termed ***K*** – is assembled and the selected boundary conditions are applied. The minimization of the total potential energy is then ensured by solving the equation ***F=KU***, where ***F*** is the vector of nodal forces and ***U*** the vector of nodal displacements. This approach based on the use of BBe elements takes the advantage of the flexibility of the FE method and allows for the semi-analytical resolution of the bonded overlap system of differential equations at low computational costs. Using BBe elements as elementary bricks of larger models then offers the possibility to simulate more complex structures involving single-lap bonded joints at low computational costs (Stapelton 2012).

2.2. Formulation of the BBe element

2.2.1. Hypotheses. The model is based on the following hypotheses: (i) the thickness of the adhesive layer is constant along the overlap, (ii) the adherends are simulated by linear elastic Euler-Bernoulli laminated beams, and (iii) the adhesive layer is simulated by an infinite number of elastic shear and peel springs supporting both adherends interfaces.

2.2.2. Governing differential equations. The local equilibrium of both adherends (see Fig.1) leads to the following system of six equations:

$$\begin{cases} \dfrac{dN_j}{bdx} = (-1)^j T \\ \dfrac{dV_j}{bdx} = (-1)^{j+1} S \qquad , \quad j = 1,2 \\ \dfrac{dM_j}{dx} + V_i + \dfrac{1}{2}(e_j + e)bT = 0 \end{cases} \tag{1}$$

where S is the adhesive peel stress, T the adhesive shear stress, N_1 (N_2) the normal force in adherend 1 (2), V_1 (V_2) the shearing force in adherend 1 (2) and M_1 (M_2) the bending

ACCEPTED MANUSCRIPT

moment in adherend 1 (2). Note that equation (1) refers to the local equilibrium derived and employed in (Goland & Reissner 1944).

Considering the possible extensional and bending coupling stiffnesses in the adherends, the constitutive equations are expressed as:

$$\begin{cases} N_j = A_j \dfrac{du_j}{dx} - B_j \dfrac{d^2 w_j}{dx^2} \\ M_j = -B_j \dfrac{du_j}{dx} + D_j \dfrac{d^2 w_j}{dx^2}, \quad j = 1,2 \\ \theta_j = \dfrac{dw_j}{dx} \end{cases} \tag{2}$$

with A_j the extensional stiffness, B_j the coupling stiffness, and D_j the bending stiffness of adherend j ($j=1,2$). Further details on these constitutive equations can be found in standard textbooks on composite mechanics (Jones 1998, Berthelot 1999) and in Appendix.1. Note that assuming isotropic material the given relations can be reduced to:

$$\begin{cases} A_j = bE_j e_j \\ B_j = 0 \\ D_j = b E_j e_j^3 / 12 \end{cases}, \quad j = 1,2 \tag{3}$$

For simplification purpose, the described theory has been here voluntarily restricted to the Kirchhoff-Love assumptions (i.e. Classical Laminate Theory). However the adherend shear stress can possibly be assumed as varying linearly with the adherend thickness (Paroissien *et al.* 2013). For demonstration purpose it is assumed that $\Delta_j = A_j D_j - B_j^2$ is not equal to zero.

The adhesive is considered as linear elastic and is simulated by an infinite number of elastic shear and elastic peel springs. The adhesive shear and peel stresses are then expressed as:

$$\begin{cases} T = \dfrac{G}{e}\left(u_2 - u_1 - \dfrac{1}{2} e_1 \theta_1 - \dfrac{1}{2} e_2 \theta_2 \right) \\ S = \dfrac{E}{e}\left(w_1 - w_2 \right) \end{cases} \tag{4}$$

ACCEPTED MANUSCRIPT

where E refers to the *peel modulus* of the adhesive (see Appendix.2), G the shear modulus of the adhesive, u_1 (u_2) the normal displacement of adherend 1 (2), w_1 (w_2) the transverse deflection of adherend 1 (2), and θ_1 (θ_2) the bending angle of adherend 1 (2).

2.2.3. Stiffness matrix of the BBe element.

System of differential equations in terms of adhesive stresses. From equation (2) falls:

$$\begin{cases} \dfrac{du_j}{dx} = \dfrac{D_j N_j + B_j M_j}{\Delta_j} \\ \dfrac{d^2 w_j}{dx^2} = \dfrac{A_j M_j + B_j N_j}{\Delta_j} \end{cases}, j = 1,2 \qquad (5)$$

By combining equations (1) (2) (4) and (5), the following linear differential equation system in terms of adhesive stresses is obtained:

$$\begin{cases} \dfrac{d^3 T}{dx^3} = k_1 \dfrac{dT}{dx} + k_2 S \\ \dfrac{d^4 S}{dx^4} = -k_4 S - k_3 \dfrac{dT}{dx} \end{cases} \qquad (6)$$

where:

$$\begin{cases} k_1 = \dfrac{Gb}{e}\left[\dfrac{D_1}{\Delta_1}\left(1 + \dfrac{A_1 e_1 (e_1 + e)}{4D_1}\right) + \dfrac{D_2}{\Delta_2}\left(1 + \dfrac{A_2 e_2 (e_2 + e)}{4D_2}\right) + \left(\dfrac{e_1 B_1}{\Delta_1} + \dfrac{eB_1}{2\Delta_1} - \dfrac{e_2 B_2}{\Delta_2} - \dfrac{eB_2}{2\Delta_2}\right)\right] \\ k_2 = \dfrac{Gb}{e}\left[\dfrac{e_1 A_1}{2\Delta_1} - \dfrac{e_2 A_2}{2\Delta_2} + \left(\dfrac{B_1}{\Delta_1} + \dfrac{B_2}{\Delta_2}\right)\right] \\ k_3 = \dfrac{Eb}{e}\left[\dfrac{(e_1 + e)A_1}{2\Delta_1} - \dfrac{(e_2 + e)A_2}{2\Delta_2} + \left(\dfrac{B_1}{\Delta_1} + \dfrac{B_2}{\Delta_2}\right)\right] \\ k_4 = \dfrac{Eb}{e}\left[\dfrac{A_1}{\Delta_1} + \dfrac{A_2}{\Delta_2}\right] \end{cases} \qquad (7)$$

ACCEPTED MANUSCRIPT

ACCEPTED MANUSCRIPT

By successive differentiations and linear combinations, the system of differential equations (6) can be uncoupled as:

$$\begin{cases} \dfrac{d^6S}{dx^6} - k_1\dfrac{d^4S}{dx^4} + k_4\dfrac{d^2S}{dx^2} + S(k_2k_3 - k_1k_4) = 0 \\ \dfrac{d}{dx}\left(\dfrac{d^6T}{dx^6} - k_1\dfrac{d^4T}{dx^4} + k_4\dfrac{d^2T}{dx^2} + T(k_2k_3 - k_1k_4)\right) = 0 \end{cases} \tag{8}$$

The system (8) is then solved with respect to the classical theory of homogeneous differential equations, and the adhesive shear and peel stresses are expressed as:

$$\begin{cases} S(x) = \begin{bmatrix} \overline{K_1}e^{sx}\sin(tx) + \overline{K_2}e^{sx}\cos(tx) + \overline{K_3}e^{-sx}\sin(tx) \\ + \overline{K_4}e^{-sx}\cos(tx) + \overline{K_5}e^{rx} + \overline{K_6}e^{-rx} \end{bmatrix} \\ T(x) = \begin{bmatrix} K_1e^{sx}\sin(tx) + K_2e^{sx}\cos(tx) + K_3e^{-sx}\sin(tx) \\ + K_4e^{-sx}\cos(tx) + K_5e^{rx} + K_6e^{-rx} + K_7 \end{bmatrix} \end{cases} \tag{9}$$

Nodal displacements and forces. The determination of the stiffness matrix of BBe element requires the determination of both the nodal displacements and the nodal forces (see Fig.2). Following the resolution scheme introduced in (Hogberg 2004), the displacements (forces) in each adherend are expressed as functions of both the adhesive stresses and their respective derivatives. The computation of the displacements (forces) of each adherend is fully detailed in (Paroissien *et al.* 2013). However it is shown that the entire problem is dependent on a total number of 12 integration constants only:

$${}^{t}\mathrm{C} = \begin{pmatrix} K_1 & K_2 & K_3 & K_4 & K_5 & K_6 & K_7 & J_1 & J_2 & J_3 & J_5 & J_7 \end{pmatrix} \tag{10}$$

The nodal displacements (forces) are then computed from the values of displacements (forces) at $x=0$ and $x=\Delta$. It is shown that the nodal displacements (forces) are linearly dependent on the 12 integration constants listed in (10), through a coupling parameter matrix $\boldsymbol{M}$ ($\boldsymbol{N}$):

ACCEPTED MANUSCRIPT

$$\mathbf{U}=\begin{pmatrix} u_i \\ u_j \\ u_k \\ u_l \\ w_i \\ w_j \\ w_k \\ w_l \\ \theta_i \\ \theta_j \\ \theta_k \\ \theta_l \end{pmatrix} = \begin{pmatrix} u_1(0) \\ u_2(0) \\ u_1(\Delta) \\ u_2(\Delta) \\ w_1(0) \\ w_2(0) \\ w_1(\Delta) \\ w_2(\Delta) \\ \theta_1(0) \\ \theta_2(0) \\ \theta_1(\Delta) \\ \theta_2(\Delta) \end{pmatrix} = \mathbf{MC} \quad \textit{and} \quad \mathbf{F}=\begin{pmatrix} Q_i \\ Q_j \\ Q_k \\ Q_l \\ R_i \\ R_j \\ R_k \\ R_l \\ S_i \\ S_j \\ S_k \\ S_l \end{pmatrix} = \begin{pmatrix} -N_1(0) \\ -N_2(0) \\ N_1(\Delta) \\ N_2(\Delta) \\ -V_1(0) \\ -V_2(0) \\ V_1(\Delta) \\ V_2(\Delta) \\ -M_1(0) \\ -M_2(0) \\ M_1(\Delta) \\ M_2(\Delta) \end{pmatrix} = \mathbf{NC} \tag{11}$$

where *Q*, *R* and *S* respectively refer to the nodal normal forces, shearing forces and bending moments acting onto the edges of the bonded overlap (i.e. nodes *i,j,k,l*).

Stiffness matrix. Classically, the coefficients of the stiffness matrix are obtained by differentiating each component of the nodal forces by each component of the nodal displacements:

$$\mathbf{K}_{\mathbf{BBe}}=\begin{pmatrix} \left[\frac{\partial Q_\sigma}{\partial u_\tau}\right] & \left[\frac{\partial Q_\sigma}{\partial w_\tau}\right] & \left[\frac{\partial Q_\sigma}{\partial \theta_\tau}\right] \\ \left[\frac{\partial R_\sigma}{\partial u_\tau}\right] & \left[\frac{\partial R_\sigma}{\partial w_\tau}\right] & \left[\frac{\partial R_\sigma}{\partial \theta_\tau}\right] \\ \left[\frac{\partial S_\sigma}{\partial u_\tau}\right] & \left[\frac{\partial S_\sigma}{\partial w_\tau}\right] & \left[\frac{\partial S_\sigma}{\partial \theta_\tau}\right] \end{pmatrix} \quad ,\sigma,\tau = i,j,k,l \tag{12}$$

so that:

$$\mathbf{F}=\mathbf{K}_{\mathbf{BBe}}\mathbf{U} \tag{13}$$

But, considering the expression for the vector of nodal forces (***F***) as a function of the vector of integration constants (***C***) as well as the vector ***C*** as a function of the vector of nodal displacements (***U***), the stiffness matrix of the BBe element can be computed as follows:

$$\mathbf{K}_{\mathbf{BBe}}=\mathbf{N}\mathbf{M}^{-1} \tag{14}$$

ACCEPTED MANUSCRIPT

ACCEPTED MANUSCRIPT

2.2.4. Stiffness matrix of the outer adherends and assembly of the entire structure.

The equations of local equilibrium of beams outside the overlap are written as follows:

$$\begin{cases} \dfrac{dN_j}{dx} = 0 \\ \dfrac{dV_j}{dx} = 0 \\ \dfrac{dM_j}{dx} + V_i = 0 \end{cases} , j = 1,2 \qquad (15)$$

These equations are the ones derived and employed within the classical Euler-Bernoulli beam theory.

In addition to the constitutive equations of adherends (equation (2)), the stiffness matrix of a beam element – denoted $\boldsymbol{K_{Beam}}$ – can be computed following the same method as the one presented for the BBe element (see Section.2). The stiffness matrix of the outer adherend element can then be written as follows:

$$\mathbf{K}_{\mathbf{Beam}} = \begin{pmatrix} \frac{A_j}{l_j} & -\frac{A_j}{l_j} & 0 & 0 & -\frac{B_j}{l_j} & \frac{B_j}{l_j} \\ -\frac{A_j}{l_j} & \frac{A_j}{l_j} & 0 & 0 & \frac{B_j}{l_j} & -\frac{B_j}{l_j} \\ 0 & 0 & \frac{12}{l_j^3}\frac{\Delta}{A_j} & -\frac{12}{l_j^3}\frac{\Delta}{A_j} & \frac{6}{l_j^2}\frac{\Delta}{A_j} & \frac{6}{l_j^2}\frac{\Delta}{A_j} \\ 0 & 0 & -\frac{12}{l_j^3}\frac{\Delta}{A_j} & \frac{12}{l_j^3}\frac{\Delta}{A_j} & -\frac{6}{l_j^2}\frac{\Delta}{A_j} & -\frac{6}{l_j^2}\frac{\Delta}{A_j} \\ -\frac{B_j}{l_j} & \frac{B_j}{l_j} & \frac{6}{l_j^2}\frac{\Delta}{A_j} & -\frac{6}{l_j^2}\frac{\Delta}{A_j} & \frac{1}{l_j}\left(3\frac{\Delta}{A_j}+D_j\right) & \frac{1}{l_j}\left(3\frac{\Delta}{A_j}-D_j\right) \\ \frac{B_j}{l_j} & -\frac{B_j}{l_j} & \frac{6}{l_j^2}\frac{\Delta}{A_j} & -\frac{6}{l_j^2}\frac{\Delta}{A_j} & \frac{1}{l_j}\left(3\frac{\Delta}{A_j}-D_j\right) & \frac{1}{l_j}\left(3\frac{\Delta}{A_j}+D_j\right) \end{pmatrix} , j = 1,2 \qquad (16)$$

The stiffness matrix of the entire structure – termed $\boldsymbol{K}$ – is then assembled from both the elementary stiffness matrix $\boldsymbol{K_{BBe}}$ and the elementary stiffness matrix $\boldsymbol{K_{Beam}}$ according to the classical FE assembly rules (see Fig.3).

2.3. Comparison with existing sandwich-type models

ACCEPTED MANUSCRIPT

Numbers of sandwich analyses of adhesively bonded joints can be found in the open literature (Williams 1975, Bigwood & Crocombe 1991, Hogberg 2004, Weissgraeber 2014). Those analyses, and generally referred as sandwich-type analyses, allow for the resolution of the set of governing differential equations from both the knowledge of the forces acting onto the edges of the bonded overlap and the material (and geometrical) properties of the bonded overlap. However those analyses apply to linear-elastic deformations of the sandwich structure only.

In Fig.5 is presented a comparison between the suggested approach and the Weissgraeber's sandwich-type model in terms of adhesive shear stress (a) and adhesive peel stress (b) distributions along the overlap in the case of linear elastic solicitations. The geometry parameters and material properties are given in Fig.4. To allow for the comparison of comparable results, the extensional and bending stiffnesses of the macro-element were computed from the plane-stress adherends Young's moduli as follows:

$$E_j^* = E_j / \left(1 - \nu_j^2\right) \tag{17}$$

Where E_j and ν_j respectively refer to the Young's modulus and the Poisson's ratio of adherends j ($j=1,2$) and determined from bulk material properties.

It is shown from Fig.5 that even if in close agreement, the results obtained from the suggested approach are not literally equivalent to those of the Weissgraeber's theory. These differences between the two models come from the less restrictive hypotheses of the Weissgraeber's theory. Indeed, in his original theory Weissgraeber did not limited the behavior of the adherends to the classical Kirchhoff-Love assumptions and included the effect of the possible rotation between the cross section and the bending line (then leading to the addition of a second order derivative of the peel stress in equations (6a) and (6b)) and included the effect of the adhesive thickness onto the joint equilibrium equations.

However, and due to its sandwich-type formulation, the Weissgraeber's model is limited by the need to evaluate the forces acting onto the overlap edges in advance of the sandwich analysis. Then simplifying the adhesive joint behaviour to allow for the a priori

ACCEPTED MANUSCRIPT

evaluation of the forces acting onto the edges of the sandwich structure. In the suggested approach, the outer adherends are assumed as behaving as classical Euler-Bernoulli beams (i.e. leading to the formulation of specific beam elements (see Section.2.2.4)). The resolution of the governing differential equations is then ensured by the minimization of the total potential energy (i.e. solving equation ***F=KU***, where ***F*** is the vector of nodal forces, ***U*** the vector of nodal displacements, and ***K*** the specifically formulated stiffness matrix of the entire structure). Then the forces acting onto the edges of the overlap have not to be evaluated in advance of the sandwich analysis, but lie from the resolution procedure itself. Then allowing for the modeling of various combinations of BBe and beam elements at low computational costs.

2.4. Comparison with Finite Element Analyses

The Finite Element (FE) method is a computational procedure which allows for the approximate solution of various engineering problems to be numerically assessed. The stress analysis of adhesively bonded joints is one of these problems. Although this general procedure is computationally expansive and can lead to numerical convergence issues (i.e. the mesh of adhesive layers has to be intensively refined to capture the local stress gradient at bondline edges), the FE method allows for the study of various joint geometries (e.g. various adherends geometries, variations in the adhesive thickness, etc.).

Here is presented a comparison in terms of adhesive peel stress and adhesive shear stress distributions between the results obtained from the suggested semi-analytical procedure and those of 2D Finite Element Analyses (FEA). The comparison is performed in the case of linear elastic solicitations and applies to *SLJ* configurations only. The specimen geometry as well as the material properties are given in Fig.6. The adhesive bondline is modelled using cohesive interface elements.

ACCEPTED MANUSCRIPT

It is seen from Fig.7 that the semi-analytical results are in close agreement with those of 2D FE Analyses for various adherends thickness/length ratios (e.g. 1/60, 3/60, 6/60, 9/60, 12/60 and 15/60).

3. SEMI-ANALYTICAL COHESIVE ZONE MODELING

In this section, the adhesive layer is assumed to have a non-linear behavior. To take into account the non-linear behavior of the adhesive layer, an iterative procedure derived from the classical FE theory (Crisfield 1991, Borst *et al.* 2012, Abbas 2013) is presented. The possible mixed-mode I/II response of various non-linear adhesive behaviors is then addressed through an extension of the classical CZM procedure (Valoroso 2004, De Moura 2008, Campilho 2013, Anyfantis 2012). This procedure allows for various non-linear adhesive behaviors and (or) mixed-mode criteria to be accounted for with no restriction on the specimen geometry.

3.1. Mixed-mode modeling

In the present paper, a particular emphasis is given to the modeling of 3 softening and 1 perfectly plastic adhesive behaviors (see Fig.8). However the given procedure is not limited to these particular behaviors only, and can easily applies to coupled elasto-plasto-damaging behaviors. For convenience, the adhesive stress-strain relationship is thereafter referred as the adhesive traction-separation law.

3.1.1. Description of the mixed-mode I/II adhesive behavior. Because of the 1D-beam foundation of the BBe element system of governing differential equations, it is necessary to account for the possible mixed-mode I/II response of the adhesive layer. The mixed-mode I/II response of such material models can be accounted for through the definition of the following parameters:

ACCEPTED MANUSCRIPT

$$\begin{cases} \beta = \dfrac{\delta_{II}}{\delta_{I}} \\ \delta_{m} = \sqrt{\delta_{I}^{2} + \delta_{II}^{2}} \end{cases} \tag{18}$$

where β, δ_I, δ_{II}, δ_m, respectively refer to the mixed-mode ratio, the peeling deformation, the shearing deformation and the mixed-mode deformation of the adhesive layer. A schematic representation of those parameters is given in Fig.9.

3.1.2. Description of the pure modes adhesive behavior. The basic idea of mixed-mode modeling is to combine pure mode traction-separation laws through both initiation and propagation criteria. The effective properties of the adhesive layer when facing mixed-mode deformations are then computed with respect to those initiation and propagation criteria. Numbers of those criteria can be found in the open literature (see Tab.1). To allow for the combination of the pure mode traction-separation laws, both the elastic energy (Y_{0i}) and the fracture energy (G_{Ci}) of pure modes i (i=I,II) are generally required. A mathematical description of such pure modes is then needed (see Tab.2-3).

3.1.3. Combination of the pure modes adhesive behavior. To compute the effective properties of the pure mode traction separation laws, both the elastic energy ($Y_{0,mi}$) and fracture energy ($G_{C,mi}$) of the pure mode projections of the mixed-mode traction-separation law have to be computed (see Fig.9). Since the shape of the projected traction-separations laws is assumed as identic as the initial pure mode traction-separation laws, the elastic and fracture energies of the projected traction-separation laws ($Y_{0,mi}$, $G_{C,mi}$) can be derived from the expression of the pure mode elastic and fracture energies ($Y_{0,i}$, $G_{C,i}$) by changing the subscript i in mi. Considering the projected elastic and fracture energies ($Y_{0,mi}$, $G_{C,mi}$) as a function of the effective pure mode traction-separation thresholds ($\delta_{0,mi}$, $\delta_{C,mi}$), both initiation/propagation criteria can be expressed in the form of:

$$F_k\left(\delta_{0,mi}, \delta_{C,mi}, k_i, \delta_{0,i}, \delta_{C,i}, \beta\right) = 0 \quad \begin{matrix} ,i = I, II \\ ,k = 0, C \end{matrix} \tag{19}$$

ACCEPTED MANUSCRIPT

where $F_k(\delta_{0,mi},\delta_{C,mi},k_i,\delta_{0,i},\delta_{C,i},\beta)$ refers to a function of the effective initiation/propagation thresholds ($\delta_{0,mi}$, $\delta_{C,mi}$), the mixed-mode ration (β), and the initial pure mode properties (k_i, $\delta_{0,i}$, $\delta_{C,i}$).

Since simple algebraic expressions of the effective initiation/propagation thresholds cannot be always written (Anyfantis 2012), an iterative procedure based on the false position method is derived to compute those pure mode projections of the mixed-mode traction-separation law. Assuming two initial sets of physically acceptable test values (***a***, ***b***), the solution of the problem $F_k(\delta_{0,mi},\delta_{C,mi},k_i,\delta_{0,i},\delta_{C,i},\beta)=0$ is iteratively approached using the root of the secant line between $(\boldsymbol{a}, F(\boldsymbol{a}))$ and $(\boldsymbol{b}, F(\boldsymbol{b}))$ (see Fig.10). The given procedure allows for the effective pure mode properties ($\delta_{0,mi}$, $\delta_{C,mi}$) for various non-linear adhesive stress-strain evolution laws and (or) various initiation/propagation criteria, to be computed from both the mixed-mode ratio (β) and the initial pure mode properties (k_i, $\delta_{0,i}$, $\delta_{C,i}$).

3.2. Non-linear iterative convergence scheme

3.1.1. Overview of the Newton-Raphson procedure. The Newton-Raphson procedure is a numerical procedure which allows for the root of non-linear equations to be iteratively approached. The method consists in building a vector series $\boldsymbol{X}^n$ converging towards the solution $\boldsymbol{X}$ of a non-linear problem $F(\boldsymbol{X})=0$. To allow for the next iteration $\boldsymbol{X}^{n+1}$ to be computed from the knowledge of $\boldsymbol{X}^n$, the function $F(\boldsymbol{X})$ is approached by its first order Taylor expansion around $\boldsymbol{X}^n$ such that:

$$0 \approx F\left(\mathbf{X}^{n+1}\right) = F\left(\mathbf{X}^{n}\right) + F'\left(\mathbf{X}^{n}\right)\left(\mathbf{X}^{n+1} - \mathbf{X}^{n}\right) \tag{20}$$

Assuming $\boldsymbol{X}^{n+1}$ as satisfying $F(\boldsymbol{X}^{n+1})\approx 0$, the next iteration $\boldsymbol{X}^{n+1}$ can be computed as follows:

$$\mathbf{X}^{n+1} = \mathbf{X}^{n} - \left[F'\left(\mathbf{X}^{n}\right)\right]^{-1} F\left(\mathbf{X}^{n}\right) \tag{21}$$

Where $F'(\boldsymbol{X})$ refers to the tangent linear application associated with the function $F(\boldsymbol{X})$. Then, the exact value of $F(\boldsymbol{X}^{n+1})$ is recomputed and the function $F(\boldsymbol{X})$ relinearized using

ACCEPTED MANUSCRIPT

its first order Taylor expansion around $\boldsymbol{X}^{n+1}$. The given procedure is then repeated until the difference between two following iterations falls below a given convergence criterion. The recomputation of $F(\boldsymbol{X}^{n+1})$ is generally referred as the projection step. In the case of linear applications, the derivative $F'(\boldsymbol{X})$ is referred as the Jacobian matrix of $F(\boldsymbol{X})$ at point $\boldsymbol{X}$.

One of the greatest advantages of the Newton-Raphson procedure is that the convergence rate near to the solution $\boldsymbol{X}$ is quadratic. However, the use of this procedure requires the computation of the tangent linear application at each convergence step, implying time-consuming computations, possible divergence of the algorithm and (or) numerical issues.

Since the computation of the Newton-Raphson iteration $\boldsymbol{X}^{n+1}$ has not necessarily to be approached using the first order Taylor expansion of $F(\boldsymbol{X})$, numbers of authors suggested the use of other linear applications. These modified procedures are referred as quasi Newton-Raphson procedures.

3.1.2. Global equilibrium of the joint. Because of the FE like formulation of the BBe element, the global equilibrium of the bonded overlap can be expressed in the form of:

$$\delta\Pi = 0 = \delta\mathbf{U}^T \mathbf{K}_S \mathbf{U} - \delta\mathbf{U}^T \mathbf{F}_{ext} \tag{22}$$

where $\boldsymbol{K_S}$ refers to the secant stiffness matrix, $\boldsymbol{U}$ to the vector of nodal displacements and $\boldsymbol{F_{ext}}$ to the applied nodal forces defined in Section.2. The given equilibrium condition derives from the application of the Principle of Virtual Work and applies to each BBe element.

3.1.3. Adaptation of the Newton-Raphson procedure

Adaptation of the general Newton-Raphson procedure. As presented in the previous section, the equilibrium condition (22) applied to each BBe element. The following demonstration then refers to the equilibrium of a unique BBe element. However it can be easily extended to the entire structure using the classical FE assembly rules.

ACCEPTED MANUSCRIPT

Assuming $\delta \boldsymbol{U}^T$ as kinematically acceptable, the aforementioned equilibrium can be expressed as:

$$\mathbf{L}^{\text{int}}(\mathbf{U}) = \mathbf{L}^{\text{ext}}(\mathbf{U}) \tag{23}$$

where $\boldsymbol{L}^{int}=\boldsymbol{K}_s\boldsymbol{U}$ and $\boldsymbol{L}^{ext}=\boldsymbol{F}_{ext}$ respectively refer to the internal reactions and the external forces acting on the BBe element. Note that in the general case, both $\boldsymbol{L}^{int}$ and $\boldsymbol{L}^{ext}$ depend on the vector of nodal displacements $\boldsymbol{U}$. Considering that no *following forces*, such as load pressure or centrifugal forces, are applied to the joint, $\boldsymbol{L}^{ext}$ does not depend on the vector of nodal displacements $\boldsymbol{U}$.

The expression of the element equilibrium can then be simplified as:

$$\mathbf{L}^{\text{int}}(\mathbf{U}) = \mathbf{L}^{\text{ext}} \tag{24}$$

Defining the linear application R as the difference between $\boldsymbol{L}^{int}$ and $\boldsymbol{L}^{ext}$, the research of the solution of the element equilibrium can be reduced to the research of the root of $R(\boldsymbol{U})=0$. For convenience, the linear application $R(\boldsymbol{U})$ will be thereafter referred as the vector of imbalanced loads.

$$R(\mathbf{U}) = 0 = \mathbf{L}^{\text{int}}(\mathbf{U}) - \mathbf{L}^{\text{ext}} \tag{25}$$

The research of the solution of the non-linear problem $R(\boldsymbol{U})=0$ can thus be seen as a direct application of the Newton-Raphson procedure. Considering $\boldsymbol{U}^n$ as an increasingly better estimation of the equilibrium solution $\boldsymbol{U}$, the next iteration $\boldsymbol{U}^{n+1}$ can be computed as follows:

$$\mathbf{U}^{n+1} = \mathbf{U}^{n} - \left[R'(\mathbf{U}^{n})\right]^{-1} R(\mathbf{U}^{n}) \tag{26}$$

Within the original Newton-Raphson procedure, the tangent linear application $F'(X)$ has to be computed at each convergence iteration. In equation (26), $R'(\boldsymbol{U})$ refers to the tangent linear application associated with $R(\boldsymbol{U})$. In the absence of *following forces*, the tangent linear application $R'(\underline{\boldsymbol{U}})$ can be expressed as:

$$R'(\mathbf{U}^{n}) = \left.\frac{\partial \mathbf{L}^{\text{int}}}{\partial \mathbf{U}}\right|_{\mathbf{U}^n} - \left.\frac{\partial \mathbf{L}^{\text{ext}}}{\partial \mathbf{U}}\right|_{\mathbf{U}^n} = \left.\frac{\partial \mathbf{L}^{\text{int}}}{\partial \mathbf{U}}\right|_{\mathbf{U}^n} \tag{27}$$

ACCEPTED MANUSCRIPT

where the derivative of $\boldsymbol{L^{int}}$ refers to the Jacobian matrix of the linear application $\boldsymbol{L^{int}}=\boldsymbol{K_S U}$. Note that if *following forces* are applied to the structure, the tangent linear application *R'(**U**)* cannot be reduced to the single derivative of $\boldsymbol{L^{int}}$.

$$\left.\frac{\partial \mathbf{L}^{\mathrm{int}}}{\partial \mathbf{U}}\right|_{\mathbf{U}^n} = \left.\frac{\partial}{\partial \mathbf{U}}\mathbf{K}_{\mathrm{S}}\mathbf{U}\right|_{\mathbf{U}^n} = \begin{bmatrix} \left.\frac{\partial L_1^{\mathrm{int}}}{\partial U_1}\right|_{\mathbf{U}^n} & \cdots & \left.\frac{\partial L_1^{\mathrm{int}}}{\partial U_k}\right|_{\mathbf{U}^n} \\ & \ddots & \\ \left.\frac{\partial L_k^{\mathrm{int}}}{\partial U_1}\right|_{\mathbf{U}^n} & \cdots & \left.\frac{\partial L_k^{\mathrm{int}}}{\partial U_k}\right|_{\mathbf{U}^n} \end{bmatrix} \tag{28}$$

However, as the secant stiffness matrix $\boldsymbol{K_S}$ depends on the BBe element nodal displacement $\boldsymbol{U}$, the exact computation of the tangent linear application is not possible. It is then decided to focus on quasi Newton-Raphson procedures.

Computation of the vector of imbalanced loads. Since the exact computation of the imbalance load vector highly determines the convergence of the series $\boldsymbol{U}^n$ toward the equilibrium solution $\boldsymbol{U}$, a particular attention has to be given to its correct estimation. As previously presented, the imbalance load vector is defined as the difference between the vectors of internal reactions $\boldsymbol{L^{int}}$ and applied forces $\boldsymbol{L^{ext}}$ acting on the BBe element (equation (25)).

The vector of internal reactions $\boldsymbol{L^{int}}=\boldsymbol{K_S U}$ can then be computed from both the secant stiffness matrix $\boldsymbol{K_S}$ of the BBe element and the vector of nodal displacements $\boldsymbol{U}$. However, the secant stiffness matrix is defined on a set of constant adhesive peel and shear moduli (see Section.2). Since the projection of the adhesive stresses can lead to dissimilar left side and right side adhesive secant stiffnesses (see Fig.11), it is decided to update the secant stiffness matrix using the averaged peel and shear moduli along the element.

The vector $\boldsymbol{L^{ext}}=\boldsymbol{F_{ext}}$ can in turn be computed from the external forces applied to the BBe element. Using the definition of the secant stiffness matrix $\boldsymbol{K_S}$, $\boldsymbol{L^{ext}}$ can be expressed from the secant stiffness matrix at iteration $\boldsymbol{U}^{n-1}$ and the vector of the BBe element nodal displacements at iteration $\boldsymbol{U}^n$.

ACCEPTED MANUSCRIPT

Finally, the vector of imbalanced loads $R(\mathbf{U})$ can be expressed in the form of:

$$R(\mathbf{U}) = \mathbf{K}_S\left(\mathbf{U}^{n-1}\right)\mathbf{U}^n - \mathbf{K}_S\left(\mathbf{U}^n\right)\mathbf{U}^n \quad (29)$$

Implementation of modified Newton-Raphson procedures. By discretizing the adhesive overlap with an adequate number of BBe element, it is then possible to address the non-linear response of the adhesive layer so that:

1. Initialization of the first iteration of the vector of nodal displacements ($\boldsymbol{U}=\boldsymbol{0}$)
2. Computation of the initial elastic stiffness matrix of each element
3. Assembly of the initial elastic stiffness matrix of the entire structure ($\boldsymbol{K}$)
4. Assembly of the vector of applied loads ($\boldsymbol{F}$)
5. Initialization of the vector of imbalanced loads ($\boldsymbol{R}=-\boldsymbol{F}$)
6. Computation of the first/next iteration of vector $\boldsymbol{U}$ ($\boldsymbol{U}^{n+1}=\boldsymbol{U}^n-\boldsymbol{K}^{-1}\boldsymbol{R}$)
7. Computation of the mixed-mode traction-separation parameters
8. Projection of the adhesive stresses (T, S) with respect to the computed effective traction-separation properties.
9. Computation of the updated secant stiffness matrix of each element
10. Assembly of the updated secant stiffness matrix of the entire structure ($\boldsymbol{K}$)
11. Computation of the updated vector of imbalanced loads ($\boldsymbol{R}$)

(Repeat steps 6 to 11 until a specified convergence criterion is satisfied)

4. COMPARISON WITH FINITE ELEMENT PREDICTIONS

4.1. Description of the Finite Element models

The mechanical response of three adhesive joint specimens is here investigated (*ENF*, *DCB* & *MMB*). Those specimens are characteristic of pure mode I, pure mode II and mixed-mode adhesive solicitations, and have been widely shown as consistent with the

ACCEPTED MANUSCRIPT

experimental characterization of adhesive interfaces (Kenane 1997, Reeder 1992). A schematic representation of each specimen is presented in Fig.12. The geometry of each specimen is balanced. The simulations are performed using SAMCEF FE Code v14-1.02. Both adherends are modeled as facing purely linear elastic deformations only (see Tab.4). The adhesive layer is modeled using a bi-linear cohesive traction-separation law. Both linear energetic initiation and propagation criteria are assumed (see Tab.5).

The adherends are meshed using 2D brick SAMCEF type T008 elements. The degree of each element is 1. SAMCEF type T008 elements have linear interpolation functions and 9 internal modes (ie. 8 nodes and 24 degrees of freedom). The normal integration scheme is chosen. The adhesive interface is meshed using 2D cohesive interface SAMCEF type T146 elements. The degree of each element is 1. SAMCEF type T146 elements have linear interpolation functions and no internal modes (ie. 4 nodes and 8 degrees of freedom). Because of numerical convergence issues, the Gauss-Lobatto integration scheme is here chosen (Samcef 2013). Loads and boundary conditions are applied to the neutral fiber of each adherend.

To address the complete non-linear response of the adhesive specimen when subjected to steadily increasing loads, it is firstly decided to focus on what will be thereafter referred as the load/displacement instability point. This point refers to the instant t when the structure faces the maximum level of the applied load that can be transferred to the structure (i.e. very top of the load vs displacement curve). This choice is made since the distributions of the adhesive peel stress and the adhesive shear stress at this particular moment are characteristic of the structure itself and refers to the maximum level of material nonlinearities that faces the adhesive layer during the initiation phase. To address this particular point during the specimen load history, a load based Newton-Raphson resolution procedure is employed in both FE and semi-analytical analyses (i.e. resolution procedure that stops as early as the maximum level of applicable load is reached). However the precision in reaching this particular point is directly (and highly) determined by the arbitrary fixed convergence threshold (i.e. then leading to numerical instability due to the varying maximum load reached by the Newton-Raphson procedure).

ACCEPTED MANUSCRIPT

It is then decided to evaluate the adhesive peel stress and adhesive shear stress distribution at a slightly decreased maximum load (i.e. 95% of the specimen maximum load bearing capability).

4.2. Convergence of the Finite Element models

To allow for the comparison of converged results, the mesh of each FE models is optimized so that the solution obtained is independent on its refinement. The optimization of the mesh is based on the following hypotheses: (i) the mesh of the specimen is uniformly distributed over the length, the width and the thickness of the adherends, (ii) the mesh of the upper adherend, the adhesive interface, and the lower adherend are corresponding, (iii) the aspect ratio of each element of the structure is equal to 1. It is shown from hypotheses (i) to (iii) that the mesh of the entire specimen is then dependent on the number of elements within the length of the adhesively bonded overlap only (see Appendix.3).

4.3. Description of the semi-analytical models

A schematic representation of the semi-analytical models is presented in Fig.13. The adhesive overlap is meshed using *n* uniformly distributed BBe elements. Each outer adherend is meshed using a unique and specifically formulated beam element (see Section.2.2.4). Both adherends are modeled as monolithic beams. The adhesive layer is modeled using a bi-linear cohesive traction-separation law. Both linear energetic initiation and propagation criteria are assumed (see Tab.5).

4.4. Convergence of the semi-analytical models

As presented in Section.2, when facing purely linear elastic deformations, the adhesive overlap can be modeled using a unique 4-nodes BBe element. However, the

ACCEPTED MANUSCRIPT

aforementioned procedure needs the adhesive overlap to be meshed with an adequate number of BBe elements to address the correct non-linear behavior of the adhesive layer. Since the adhesive overlap has to be meshed, the results obtained can depend on its refinement. To allow for the comparison of converged results, the semi-analytical overlap mesh is then optimized so that the solution obtained is independent on its refinement (see Appendix.3).

4.5. Comparison with Finite Element predictions

The End-Notched Flexure specimen. Fig.14 presents the comparison between semi-analytical results and Finite Element predictions in term of load versus displacement curve (a), distribution of adhesive stresses (b) and distribution of the damage variable (c) along the overlap. Fig.14-(d) then presents the *normalized deviation* between semi-analytical and Finite Element predictions. Good agreement is shown.

The Double Cantilever Beam specimen. Fig.15 presents the comparison between semi-analytical results and Finite Element predictions in term of load versus displacement curve (a), distribution of adhesive stresses (b) and distribution of the damage variable (c) along the overlap. Fig.15-(d) then presents the *normalized deviation* between semi-analytical and Finite Element predictions. Good agreement is shown.

The Mixed-Mode Bending specimen. Fig.16 presents the comparison between semi-analytical results and Finite Element predictions in term of load versus displacement curve (a), distribution of adhesive stresses (b) and distribution of the damage variable (c) along the overlap. Fig.16-(d) then presents the *normalized deviation* between semi-analytical and Finite Element predictions. Good agreement is shown.

6. DISCUSSION

ACCEPTED MANUSCRIPT

Within the present paper, an original procedure derived from the classical FE method is adapted to the particular formulation of the BBe element. Since the original approach suggested by (Paroissien *et al.* 2013) does not use the concept of shape matrix (the nodal displacements are not approximated but lies from the exact resolution of the set of the adhesive joint governing equations (see Section.2)), specific calculations have to be performed to account for the possible non-linear behavior of the adhesive layer. Then an original procedure allowing for the non-linear behavior of the adhesive layer to be accounted for (procedure derived from the classical FE method) is adapted to the particular formulation of the BBe element. The main originality of the presented Newton-Raphson iteration procedure lies in the use of the secant stiffness properties to define the non-linear problem. The vector of imbalanced loads (resulting from the projection of the non-linear adhesive stresses) is thus computed through the knowledge of the adhesive secant stiffness properties only. The suggested procedure then allows for various non-linear adhesive behaviors to be accounted for (ie. softening, plastic, etc.) with no restriction on the specimen geometry. Note that the procedure has been recently adapted to allow for the non-linear behavior of the adhesive layer as well as the non-linear behavior of each adherend to be simultaneously addressed.

In a second part, a general procedure allowing for the effective mixed-mode I/II properties of the adhesive layer to be accounted for is presented. A particular attention is given to the modeling of 3 types of cohesive damage and 1 perfectly plastic evolution laws (see Fig.8). However the procedure is not limited to these particular behaviors only. Note that the procedure has been recently adapted to coupled elasto-plastic-damaging behaviors and extended to user-defined adhesive traction-separation laws.

Finally, the mechanical response of three classical Fracture Mechanics adhesive specimens is investigated (ie. *ENF*, *DCB* and *MMB*). (Reeder 1992) and (Kenane 1997) have shown those specimens as widely used to characterize the mechanical properties of adhesive interfaces. It is seen from Fig.14-16 that semi-analytical results are in extremely close agreement with those of classical 2D Finite Element strength predictions (during both initiation and propagation phases). Indeed, the *normalized deviation*

ACCEPTED MANUSCRIPT

between Finite Elements and semi-analytical results along the overlap is shown as remaining smaller than 0.018 (shear stress), 0.06 (peel stress) and 0.04 (damage variable) for all configurations. The suggested simplified joint kinematic is then shown as consistent with the simulation of the mechanical response of those three specimens. However, and since *ENF*, *DCB* and *MMB* specimens are representative of either pure mode I, pure mode II and mixed-mode I/II adhesive solicitations, it is legitimate to think that the simplified joint kinematic will be consistent with the mechanical response of other pure mode I, pure mode II and mixed-mode I/II adhesive joint specimens, such as *bSLJ*, *IbSLJ*, *CLS*, *T-Stiff*, *V-Stiff*, etc.

When facing purely linear-elastic deformations, the semi-analytical results are shown as independent on the mesh refinement (Paroissien *et al.* 2013a). This independency on the mesh refinement due to the specific formulation of the BBe element allows for linear elastic bonded overlaps to be modeled using a unique 4-nodes BBe element. However, when facing non-linear deformations, the semi-analytical results are shown as being sensitive to this mesh refinement. To account for the non-linear behavior of the adhesive layer the adhesive overlap has then to be meshed with an adequate number of BBe elements. However, it is shown that the results obtained are rapidly converging toward an asymptote (see Fig.A3-3 and Fig.A3-4).

On the contrary, the 2D Finite Element predictions are shown as dependent on the mesh refinement in the case of both linear-elastic and non-linear adhesive deformations (see Fig.A3-5, Fig.A3-6, Fig.A3-7, and Fig.A3-8). Then, Finite Element models have to be sufficiently discretized either when locally facing elastic deformations only.

By the suggested simplified joint kinematic, it is shown that the mechanical response of a large range of bonded overlaps can be simulated using a restricted number of specifically formulated elements (i.e. only one when facing linear-elastic deformations only). Those models based on the use of BBe elements thus takes the advantage of the flexibility of FE methods (i.e. wide application range, simple assembly procedure, account for the boundary conditions, specific linear and non-linear resolution schemes, etc.) and the simplicity and robustness of theoretical approaches (i.e. analytical resolution of the set of

ACCEPTED MANUSCRIPT

governing differential equations, results independent on the mesh refinement when facing linear-elastic adhesive deformations, results shown as rapidly converging toward an asymptote when facing non-linear adhesive deformations, etc.).

Since no simplifying assumptions are made on the joint kinematic in classical 2D FE analyses, converged FE results generally imply highly refined meshes and so time-consuming computations. The suggested approach thus finds it interest in many extensive parametric (optimization) studies (procedures). It is shown from Fig.17 that the gain in terms of total number of degrees of freedom can vary from a factor 10 to 15 depending on the specimen geometry (i.e. *ENF*, *DCB* and *MMB*) and can easily be increased by a factor 3 or 4 since non-linear effects are generally limited to the close vicinity of the overlap edges (see Fig.14-16). Moreover the given procedure has been shown as 50 to 100 times quicker than equivalent 2D/3D FE predictions (Paroissien *et al.* 2013b).

Using BBe elements as elementary bricks of larger models can also be seen as an interesting solution to simulate (at low computational costs) more complex structures involving single-lap bonded overlaps Fig.18.

7. CONCLUSION

In the present paper is presented a procedure allowing for in-plane deformation adhesive joints to be simulated at low computational costs. This procedure falls from the original approach suggested by (Paroissien *et al.* 2013) and allows for various non-linear adhesive behaviors to be accounted for with no restriction on the specimen geometry. As an extension of the possible non-linear response of the structure, an extension of the classical Cohesive Zone Modeling (CZM) is proposed to allow for the mixed-mode I/II response of the adhesive layer to be addressed through various possible combinations of initiation/propagation criteria. Good agreement is shown with classical 2D Finite Element predictions, then suggesting the present model as consistent with the mechanical

ACCEPTED MANUSCRIPT

modeling (i.e. damage initiation and damage propagation) of various adhesively bonded structures.

ACKNOWLEDGMENT

G. LELIAS, E. PAROISSIEN, S. SCHWARTZ and C. GAVOILLE gratefully acknowledge the support from the SOGETI HIGH TECH engineers and managers involved in the development of JoSAT (Joint Stress Analysis Tool) internal research program. A special thanks to Mr VASSE for his help during the study of the influence of the mesh refinement on 2D/3D FE models.

ACCEPTED MANUSCRIPT

ACCEPTED MANUSCRIPT

REFERENCES

(Abbas 2013). M Abbas. Algorithm for non-linear quasi-statique analysis. R5.03.01. Code Aster. User's Manual (2013).

(Anyfantis 2012). KN Anyfantis. Analysis and design of composite-to-metal adhesively bonded joints. PhD thesis. National Technical University of Athens, School of Naval Architecture and Marine Engineering (2012).

(Berthelot 1999). JM Berthelot. Composite materials: mechanical behavior and structural analysis. New York. Springer-Verlag. (1999).

(Biel 2008). A Biel. Mechanical behavior of adhesive layers. PhD Thesis. Chalmers University of Technology, Göteborg, Sweden (2008).

(Bigwood & Crocombe 1991) DA Bigwood and AD Crocombe. Elastic analysis and engineering desing formulae for bonded joints. International J. of Adhesion and Adhesives. Vol. 9, No. 4 (1989).

(Borst *et al.* 2012). R de Borst, MA Crisfield, JCJ Remmers and CV Verhoosel. Non-linear Finite Element analysis of solids and structures. Second edition. Vol. 1. Wiley. ISBN 978-0-470-66644-9. (2012).

(Campilho 2013). RDSG Campilho, MD Benea, JABP Neto, LFM Da Silva. Modeling adhesive with cohesive zone models: effects of the cohesive law shape of the adhesive layer. Int J of Adhesion and Adhesives. Vol 44, pp. 48-56 (2013).

ACCEPTED MANUSCRIPT

ACCEPTED MANUSCRIPT

(Champaney 2004). L Champaney. Outils de conception et d'analyse pour les assemblages de structures complexes. HdR Thesis. Université de Versailles St Quentin en Yvelines (2004).

(Clarke *et al.* 2003) JLM Clarke. Structural desing of polymer composites : Eurocomp design code and background document. Second Edition. CRC Press. ISBN 0203475135. (2003).

(Crisfield 1991). MA Crisfield. Non-linear Finite Element analysis of solids and structures. Vol. 1. Wiley. ISBN 0471929565. (1991).

(Da Silva 2009). LFM da Silva, PJC das Neves, RD Adams, and JK Spelt. Analytical models of adhesively bonded joints-Part I: Literature survey. Int J Adhesion Adhesives. 29, pp. 319-330 (2009).

(Da Silva 2012). LFM da Silva, and RDSG Campilho. Advances in numerical Modelling of adhesive joints. SpringerBriefss in Applied Sciences and Technology, Publisher: Springer Berlin Heidelberg, pp. 1-93 (2012).

(De Moura 2008). MFSF de Moura, JPM Gonçalves, JAG CHOUSAL, and Campilho RDSG. Cohesive and continuum mixed-mode damage models applied to the simulation of the mechanical behavior of bonded joints. Int J Adhesion Adhesives. 28, pp. 419-426 (2008).

(Fernlund 2007). G Fernlund. Stress analysis of bonded lap joints using fracture mechanics and energy balance. Int J Solids Structures. 27, pp. 574-592 (2007).

(Fraise 1993). P Fraise and F Schimt. Use of J-integral as fracture parameter in simplified analysis of bonded joints. Int J Fracture. 63, pp. 59-73 (1993).

ACCEPTED MANUSCRIPT

(Goland & Reissner 1944). M Goland, and E Reissner. The stresses in cemented joints. J App Mech. Trans. ASME. 11, pp. A17-A27 (1944).

(Hart-Smith 1973a). RJ Hart-Smith. Adhesive-bonded single-lap joint. NASA Technical Report. CR-112236. (1973).

(Hart-Smith 1973b). RJ Hart-Smith. Adhesive-bonded double-lap joint. NASA Technical Report. CR-112235. (1973).

(Hogberg 2004). JL Högberg. Mechanical behavior of single-layer adhesive joints – An integrated approach. Thesis for the degree of licentiate of engineering. Chalmers University of Technology, Göteborg, Sweden (2004).

(Ingen 1993). JW van Ingen, and A Vlot. Stress analysis of adhesively bonded single lap joints. (Report LR-740). Delft University of Technology (April 1993).

(Kenane 1997). M Kenane, ML Benzeggagh. Mixed mode delamination fracture toughness of unidirectional glass-epoxy composites under fatigue loadings. Composite Science & Technology. Vol 57, pp. 597-605 (1997).

(Leguillon 2002). D Leguillon. Strength or toughness? A criterion for crack onset at a notch. European Journal of Mechanics-A/Solids 21 (1), pp. 61-72 (2002).

(Mortensen 1998). F Mortensen. Development of tools for engineering analysis and design of high-performance FRP-composite structural elements. PhD Thesis. Aalborg University, Denmark (1998).

(Oterkus 2004). E Oterkus, A Barut, E Madenci, SS Smeltzer III, and DR Ambur. Nonlinear analysis of bonded composite single-lap joints. Paper presented at: 45th

ACCEPTED MANUSCRIPT

AIAA/ASME/ASCE/AHS/ASC Structures, Structural Dynamics & Materials Conference, Palm Springs, CA (April 2004).

(Paroissien 2006). E Paroissien. Contribution aux assemblages hybrids. Application aux jonctions aéronautiques. PhD thesis. University of Toulouse. (2006).

(Paroissien *et al.* 2013a). E Paroissien, F Lachaud, and T Jacobs. A simplified stress analysis of bonded joints using macro-elements. In: *Advanced in Modeling and Design of Adhesively Bonded Systems*. S Kumar and KL Mittal (Eds.), Scrivener Publishing, Wiley, pp. 93-146 (2013).

(Paroissien *et al.* 2013b). E Paroissien, F Gaubert, A Da Veiga and F Lachaud. Elasto-plastic analysis of bonded joints with macro-elements. Journal of Adhesion Science and Technology. Vol 27, Issue 13, pp. 1464-1498. (2013).

(Reeder 1992). JR Reeder ; An evaluation of mixed mode delamination criteria. NASA T echnical report 104210 (1992).

(Samcef 2013). SAMCEF. SAMCEF v14.10-2. User's manual (2013).

(Stapelton 2011). SE Stapleton and AM Waas. Modeling progressive failure of bonded joints using a single joint finite elemen. AIAA Journal, Vol. 49, no. 48 (2011).

(Stapelton 2012). SE Stapleton. The analysis of adhesively bonded advanced composite joints using joint finite elements. PhD thesis. University of Michigan (2012).

(Tsai 1994). MY Tsai, and J Morton. An evaluation of analytical and numerical solutions to the single-lap joint. Int J Solids Structures. 31, pp. 2537-2563 (1994).

ACCEPTED MANUSCRIPT

(Tong 1994). L Tong. Bond shear strength for adhesive bonded double-lap joints. Int J Solids Structures. 31(21), pp. 2919-2931 (1994).

(Valoroso 2044). N Valoroso, and L Champaney. A damage model for simulating decohesion in adhesively bonded assemblies. Proceeding to ECCOMAS 2004, Jyväskyä, FI (July 2004).

(Volkersen 1938). O Volkersen. Die Nietkraftverteilung in Zugbeanspruchten Nietverbindungen mit konstanten Laschenquerschnitten. Luftfahrtforschung, Vol. 15, pp. 41-47 (1938).

(Weissgraeber 2013). P Weissgraeber and W Becker. Finite Fracture Mechanics model for mixed mode fracture in adhesive joints. Int. J Solids Structures (2013).

(Weissgraeber 2014). P Weissgraeber, N Stein and W Becker. A general sandwich-type model for adhesive joints with composite adherends. Int. J of Adhesion and Adhesives, Vol. 55, pp. 56-63 (2013).

(Williams 1975). JH Williams. Stresses in adhesive between dissimilar adherends. International J. of Adhesison and Adhesives. (1975).

ACCEPTED MANUSCRIPT

ACCEPTED MANUSCRIPT

LIST OF FIGURE CAPTIONS

Figure A2-1. Schematic representation of the relative equilibrium between the adhesive transverse deformations (due to Poisson's effects) and the reactions/oppistions of the surrounding adherends. Effective peel modulus of sandwiched adhesive layers.

Figure A3-1. Evolution of the maximum displacement at loaded nodes as a function of the number of elements within the length of the adhesive bondline. Convergence of the solution facing linear-elastic adhesive deformations. Convergence of the Finite Element Analyses.

Figure A3-2. Evolution of the adhesive peel and shear stresses at crack tip as a function of the number of elements within the length of the adhesive bondline. Convergence of the solution facing linear-elastic adhesive deformations. Convergence of the Finite Element Analyses.

Figure A3-3. Evolution of the maximum displacement at loaded nodes as a function of the number of elements within the length of the adhesive bondline. Convergence of the solution facing non-linear adhesive deformations. Convergence of the Finite Element Analyses.

Figure A3-4. Evolution of the adhesive peel and shear stresses at crack tip as a function of the number of elements within the length of the adhesive bondline. Convergence of the solution facing non-linear adhesive deformations. Convergence of the Finite Element Analyses.

Figure A3-5. Evolution of the maximum displacement at loaded nodes as a function of the number of elements within the length of the adhesive bondline. Convergence of the

ACCEPTED MANUSCRIPT

ACCEPTED MANUSCRIPT

solution facing linear-elastic adhesive deformations. Convergence of the semi-analytical models.

Figure A3-6. Evolution of the adhesive peel and shear stresses at crack tip as a function of the number of elements within the length of the adhesive bondline. Convergence of the solution facing linear-elastic adhesive deformations. Convergence of the semi-analytical models.

Figure A3-7. Evolution of the maximum displacement at loaded nodes as a function of the number of elements within the length of the adhesive bondline. Convergence of the solution facing non-linear adhesive deformations. Convergence of the semi-analytical models.

Figure A3-8. Evolution of the adhesive peel and shear stresses at crack tip as a function of the number of elements within the length of the adhesive bondline. Convergence of the solution facing non-linear adhesive deformations. Convergence of the semi-analytical models.

Figure 1. Schematic representation of the local equilibrium of the bonded adherends. Linear elastic 1D-beam model.

Figure 2. Definition of the nodal displacement (forces) acting onto the BBe element. Linear elastic 1D-beam model.

Figure 3. Assembly of the Single-Lap Joint (SLJ) configuration. Linear elastic 1D-beam model.

Figure 4. Schematic representation of the Single-Lap Joint (SLJ) adhesive specimen. Loads acting onto the sandwich edges. Comparison with existing sandwich-type models.

ACCEPTED MANUSCRIPT

ACCEPTED MANUSCRIPT

Figure 5. Comparison of the predicted adhesive shear and peel stress distributions along the overlap. Weissgraeber versus BBe. Single-Lap Joint (SLJ) configuration. Comparison with existing sandwich-type models.

Figure 6. Schematic representation of the Single-Lap Joint (SLJ) adhesive specimen. Comparison with Finite Element Analyses.

Figure 7. Comparison of the predicted adhesive shear and peel stress distributions along the overlap. Finite Element (FE) versus BBe. Single-Lap Joint configuration. Comparison with Finite Element Analyses.

Figure 8. Restriction to bi-linear (a), exponential (b), polynomial (c) and perfectly plastic (d) softening behaviors. However the procedure is not limited to these particular behaviors only. Semi-analytical cohesive zone modeling.

Figure 9. Graphical representation of the mixed-mode parameters. Description of the mixed-mode I/II adhesive behavior.

Figure 10. False position method. Computation of the effective initiation/propagation properties of the adhesive layer. Combination of the pure mode adhesive behaviors.

Figure 11. Dissimilar left side and right side adhesive secant stiffnesses. Computation of the secant stiffness matrix K_S. Adaptation of the Newton-Raphson procedure. Computation of the vector of imbalanced loads.

Figure 12. Schematic representation of the End-Notched Flexure (ENF), Double Cantilever Beam (DCB) and Mixed-Mode Bending (MMB) adhesive specimens. Description of the Finite Element (FE) models.

ACCEPTED MANUSCRIPT

ACCEPTED MANUSCRIPT

Figure 13. Schematic representation of the End-Notched Flexure (ENF), Double Cantilever Beam (DCB) and Mixed-Mode Bending (MMB) adhesive specimens. Description of the semi-analytical models.

Figure 14. Comparison between semi-analytical results and Finite Element Analyses (FEA). End-Notched Flexure (ENF) specimen. Comparison with classical Finite Element (FE) predictions.

Figure 15. Comparison between semi-analytical results and Finite Element Analyses (FEA). Double Cantilever Beam (DCB) specimen. Comparison with classical Finite Element (FE) predictions.

Figure 16. Comparison between semi-analytical results and Finite Element Analyses (FEA). Mixed-Mode Bending (MMB) specimen. Comparison with classical Finite Element (FE) predictions.

Figure 17. Comparison between semi-analytical and Finite Element (FE) predictions. Converged stress distributions. Comparison of the total number of degrees of freedom.

Figure 18. BBe eleemnts as bricks of larger models for linear and non-linear adhesive stress analyses. Discussion.

ACCEPTED MANUSCRIPT

ACCEPTED MANUSCRIPT

LIST OF TABLES

Tab 1. Examples of initiation/propagation mixed-mode criteria. Description of the pure mode adhesive behavior.

Tab 2. Mathematical representation of classical softening adhesive behaviors. Description of the pure mode adhesive behavior.

Tab 3. Mathematical description of the elastic energy ($Y_{0,i}$) and the fracture energy ($G_{c,i}$) of pure mode i (i=I,II) . Description of the pure mode adhesive behavior.

Tab 4. Adherend elastic properties. Description of the Finite Element (FE) models.

Tab 5. Adhesive cohesive properties. Description of the Finite Element (FE) models.

ACCEPTED MANUSCRIPT

ACCEPTED MANUSCRIPT

APPENDIX 1 – SUPPLEMENTARY MATERIAL ON THE ADHERENDS CONSTITUTIVE EQUATIONS

Analogously to classical Euler-Bernoulli beams theory it is possible to express the displacement field of both adherends in the form of:

$$\begin{cases} u^j(x,y) = {u_0}^j(x) - y{w_{0,x}}^j(x) \\ w^j(x,y) = {w_0}^j(x) \end{cases} \quad \text{(A3.1)}$$

Where ${u_0}^i$ and ${w_0}^i$ respectively refer to the x-axis and y-axis displacements of the neutral fiber of adherend j ($j=1,2$), and ${w_{0,x}}^i$ to the first derivative of ${w_0}^i$ with respect to x. According to the Classical Laminates Theory (CLT), it is then possible to express the axial deformation of each adherend as:

$$\varepsilon^j(x,y) = {u_{,x}}^j(x,y) = {u_{0,x}}^j(x) - y{w_{0,xx}}^j(x) \quad \text{(A3.2)}$$

And the axial stress in each ply as :

$${\sigma_k}^j(x,y) = {\overline{\mathbf{Q}}_k}^j \varepsilon^j(x,y) \quad \text{(A3.3)}$$

Where ${\overline{\mathbf{Q}}_k}^i$ refers to the reduced stiffness matrix of the k^{th} ply of adherend j ($j=1,2$). According to the Classical Laminates Theory (CLT), the normal force and the bending moment in adherend j ($j=1,2$) are expressed as:

$$\begin{cases} N_j(x) = \int_{-e_j/2}^{e_j/2} \sigma^j dydz = \sum_{k=1}^{n} \int_{y_k}^{y_{k+1}} {\sigma_k}^j dydz \\ M_j(x) = \int_{-e_j/2}^{e_j/2} \sigma^j y dydz = \sum_{k=1}^{n} \int_{y_k}^{y_{k+1}} {\sigma_k}^j y dydz \end{cases} \quad \text{(A3.4)}$$

By combining (A3-2) (A3-3) and (A3-4) it is then possible to express the normal force and the bending moment in adherend j ($j=1,2$) as:

$$\begin{cases} N_j(x) = \sum_{k=1}^{n} \int_{y_k}^{y_{k+1}} {\sigma_k}^j dydz = b\sum_{k=1}^{n} \left(\int_{y_k}^{y_{k+1}} {\overline{\mathbf{Q}}_k}^j {u_{0,x}}^j(x) dy - \int_{y_k}^{y_{k+1}} {\overline{\mathbf{Q}}_k}^j y{w_{0,xx}}^j(x) dy \right) \\ M_j(x) = -\sum_{k=1}^{n} \int_{y_k}^{y_{k+1}} {\sigma_k}^j y dydz = -b\sum_{k=1}^{n} \left(\int_{y_k}^{y_{k+1}} {\overline{\mathbf{Q}}_k}^j y{u_{0,x}}^j(x) dy - \int_{y_k}^{y_{k+1}} {\overline{\mathbf{Q}}_k}^j y^2{w_{0,xx}}^j(x) dy \right) \end{cases} \quad \text{(A3.5)}$$

ACCEPTED MANUSCRIPT

ACCEPTED MANUSCRIPT

Then leading to the adherends constitutive equations:

$$\begin{cases} N_j(x) = A_j {u_{0,x}}^j(x) - B_j {w_{0,xx}}^j(x) \\ M_j(x) = -B_j {u_{0,x}}^j(x) + D_j {w_{0,xx}}^j(x) \end{cases} \quad \text{(A3.6)}$$

Where:

$$\begin{cases} A_j = \sum_{k=1}^{n} {\overline{\mathbf{Q}}_k}^j (y_k - y_{k-1}) \\ B_j = \frac{1}{2} \sum_{k=1}^{n} {\overline{\mathbf{Q}}_k}^j \left({y_k}^2 - {y_{k-1}}^2 \right) \\ D_j = \frac{1}{3} \sum_{k=1}^{n} {\overline{\mathbf{Q}}_k}^j \left({y_k}^3 - {y_{k-1}}^3 \right) \end{cases} \quad \text{(A3.7)}$$

ACCEPTED MANUSCRIPT

ACCEPTED MANUSCRIPT

APPENDIX 2 – EFFECTIVE PEEL MODULUS OF SANDWICHED ADHESIVE LAYERS

In numbers of recent closed-form stress analyses of adhesively bonded joints (Clarke *et al.* 2003, Stapelton 2011, Stapelton 2012, Weissgraeber 2014) the adhesive layer has been assumed to act as a plane-strain deformable material when subjected to through thickness deformations. Then leading to the definition of the effective tensile adhesive modulus:

$$E_a^* = \frac{E_a(1-\nu_a)}{(1+\nu_a)(1-2\nu_a)} \quad \text{(A2.1)}$$

Where v_a refer to the adhesive Poisson's ratio and E_a to the adhesive tensile modulus determined from the bulk material properties.

This modeling of the adhesive elastic behavior when subjected to through thickness deformations lies on the assumption that when sandwiched the adhesive transverse deformations are constrained by the surrounded rigid (or semi-rigid) adherends (see Fig.A2-1). However, the adherends are in facts not infinitely rigid (especially when thin adherends are bonded). It is then legitimate to think that real adherends will allow for small adhesive transverse deformations to occur (depending on the ability of both adherends to constrain the adhesive transverse deformations). This ability of the adherends to constrain the adhesive transverse deformations can be modulated by different parameters: the thickness (or stiffness) of the surrounding adherends, the thickness (or stiffness) of the adhesive layer itself, etc.

In (Hart-Smith 1973b) the author suggested that the effective tensile modulus of the adhesive layer was resulting from a complex interaction between the adhesive layer itself and the surrounding adherends. He then suggested the use of an effective tensile modulus given by:

$$\frac{1}{E_a^*} = \frac{1}{E_a} + \frac{k_1}{E_1} + \frac{k_2}{E_2} \quad \text{(A2.2)}$$

Where E_1 and E_2 are the transverse tensile moduli of the inner and the outer adherends, k_1 and k_2 the number (or fraction) of adhesive layer thicknesses for which the adherends

ACCEPTED MANUSCRIPT

are affected by the applied peel stresses, and E_a the adhesive tensile modulus determined from the bulk material properties. He also suggested that this effective tensile modulus of the adhesive layer (equation (A1.2)) should be determined by transverse loading of an adhesive film bonded to blocks rather than from bulk material properties specimen.

Since the second definition of the adhesive tensile modulus makes more sense to the authors of the present paper, it is decided to refer to this particular modulus as the effective *peel modulus* of the adhesive layer. This *peel modulus* has then to be determined experimentally from bonded overlap specimens, and do apply to the effective tensile modulus of the adhesive layer measured when subjected to through thickness deformations.

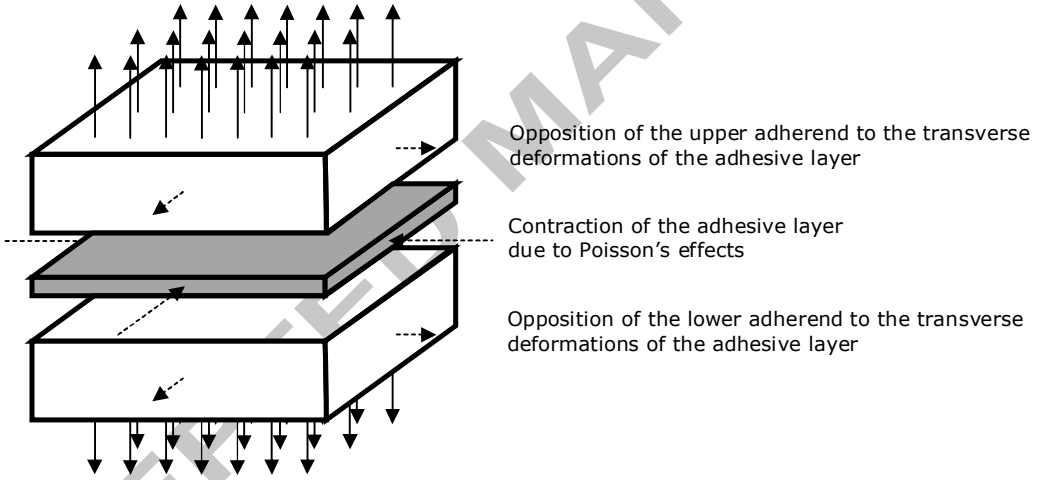


Figure A2-1. Schematic representation of the relative equilibrium between the adhesive transverse deformations (due to Poisson's effects) and the reactions/oppositions of the surrounding adherends. Effective peel modulus of sandwiched adhesive layers

ACCEPTED MANUSCRIPT

ACCEPTED MANUSCRIPT

APPENDIX 3 – CONVERGENCE OF THE NUMERICAL RESULTS

A3.1. Convergence of the Finite Element models

Convergence of the linear-elastic FE results. Since the *DCB* specimen has been largely shown as the critical configuration in term of convergence of the numerical results, the results are then presented for this configuration only. Fig.A3-1 then shows the evolution of the maximum displacement at loaded nodes as a function of the number of elements within the length of the adhesively bonded overlap of the *DCB* specimen facing linear-elastic deformations only. Fig.A3-2 shows the evolution of the adhesive peel and shear stresses at crack tip as a function of the number of elements within the length of the adhesively bonded overlap of the same specimen. It is seen from Fig.A3-1 and Fig.A3-2 that the linear elastic analyses clearly converge towards an asymptote.

Convergence of the non-linear FE results. Fig.A3-3 shows the evolution of the maximum displacement at loaded nodes as a function of the number of elements within the length of the adhesively bonded overlap of the *DCB* specimen facing non-linear adhesive deformations. Fig.A3-4 shows the evolution of the adhesive peel and shear stresses at crack tip as a function of the number of elements within the length of the adhesively bonded overlap of the same specimen. In comparison to linear elastic analyses, the non-linear solutions do not appear as clearly converging toward an asymptote (see Fig.A3-3 and Fig.A3-4). However, and since SAMCEF uses a Newton-Raphson based procedure to account for the non-linear behavior of the adhesive layer, the converged results can be noised by the inherent convergence criterion. The number of elements within the length of the overlap is then fixed to 200 for both the *ENF*, the *DCB*, and the *MMB* specimens.

A3.2. Convergence of the semi-analytical models

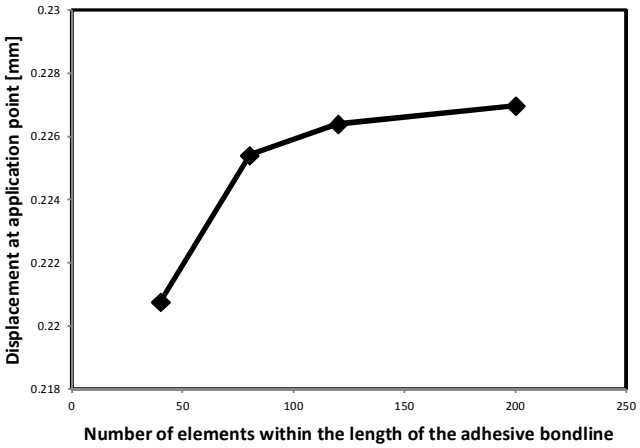
ACCEPTED MANUSCRIPT

Convergence of the linear-elastic semi-analytical results. Fig.A3-5 shows the evolution of the maximum displacement at loaded nodes as a function of the number of elements within the length of the adhesively bonded overlap of the *DCB* specimen facing linear-elastic deformations only. Fig.A3-6 shows the evolution of the adhesive peel and shear stresses at crack tip as a function of the number of elements within the length of the adhesively bonded overlap of the same specimen. It is seen from Fig.A3-5 and Fig.A3-6 that the linear elastic semi-analytical analyses are clearly independent on the mesh refinement.

Convergence of the non-linear semi-analytical results. Fig.A3-7 shows the evolution of the maximum displacement at loaded nodes as a function of the number of elements within the length of the adhesively bonded overlap of the *DCB* specimen facing non-linear adhesive deformations. Fig.A3-8 shows the evolution of the adhesive peel and shear stresses at crack tip as a function of the number of elements within the length of the adhesively bonded overlap of the same specimen. In comparison to linear elastic analyses, the non-linear solutions appear as depending on the mesh refinement. However, it is seen from Fig.A3-7 and Fig.A3-8 that the non-linear solutions rapidly converge towards an asymptote. The number of BBe elements within the length of the overlap is then fixed to 200 for both the *ENF*, the *DCB*, and the *MMB* specimens.

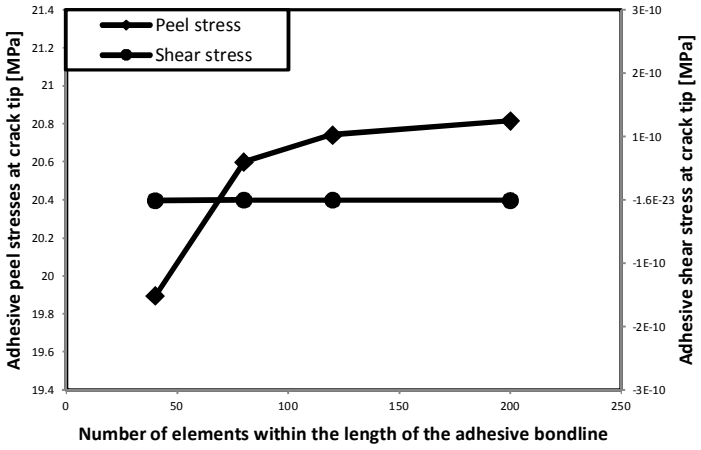
ACCEPTED MANUSCRIPT

ACCEPTED MANUSCRIPT



DCB specimen

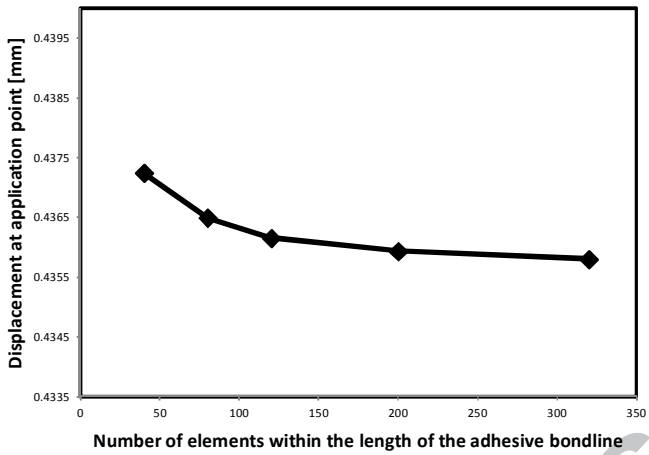
Figure A3-1. Evolution of the maximum displacement at loaded nodes as a function of the number of elements within the length of the adhesive bondline. Convergence of the solution facing linear-elastic deformations. Convergence of the Finite Element Analyses.



DCB specimen

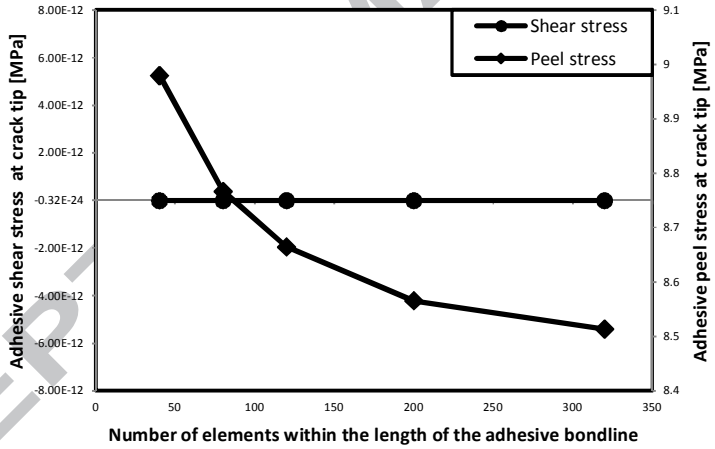
Figure A3-2. Evolution of the adhesive peel and shear stresses at crack tip as a function of the number of elements within the length of the adhesive bondline. Convergence of the solution facing linear-elastic adhesive deformations. Convergence of the Finite Element Analyses.

ACCEPTED MANUSCRIPT



DCB specimen

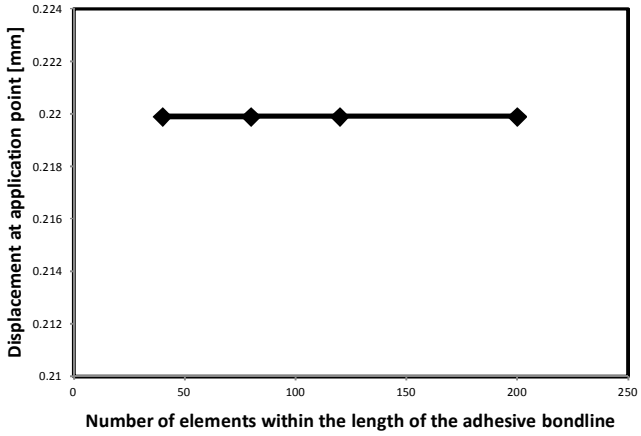
Figure A3-3. Evolution of the maximum displacement at loaded nodes as a function of the number of elements within the length of the adhesive bondline. Convergence of the solution facing non-linear adhesive deformations. Convergence of the Finite Element Analyses.



DCB specimen

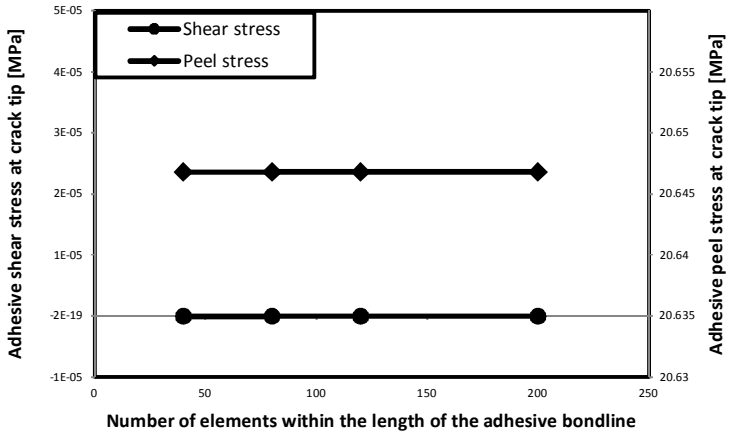
Figure A3-4. Evolution of the adhesive peel and shear stresses at crack tip as a function of the number of elements within the length of the adhesive bondline. Convergence of the solution facing non-linear adhesive deformations. Convergence of the Finite Element Analyses.

ACCEPTED MANUSCRIPT



DCB specimen

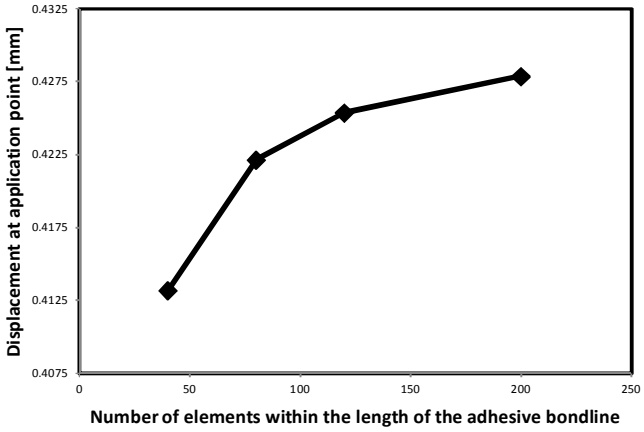
Figure A3-5. Evolution of the maximum displacement at loaded nodes as a function of the number of elements within the length of the adhesive bondline. Convergence of the solution facing linear-elastic adhesive deformations. Convergence of the semi-analytical models.



DCB specimen

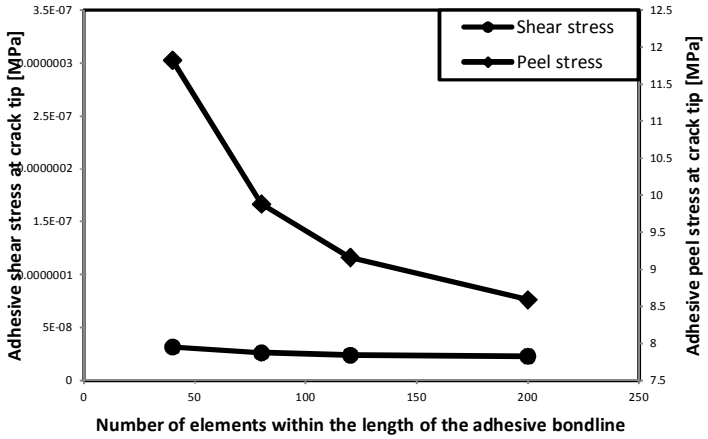
Figure A3-6. Evolution of the adhesive peel and shear stresses at crack tip as a function of the number of elements within the length of the adhesive bondline. Convergence of the solution facing linear-elastic adhesive deformations. Convergence of the semi-analytical models.

ACCEPTED MANUSCRIPT



DCB specimen

Figure A3-7. Evolution of the maximum displacement at loaded nodes as a function of the number of elements within the length of the adhesive bondline. Convergence of the solution facing non-linear adhesive deformations. Convergence of the semi-analytical models.

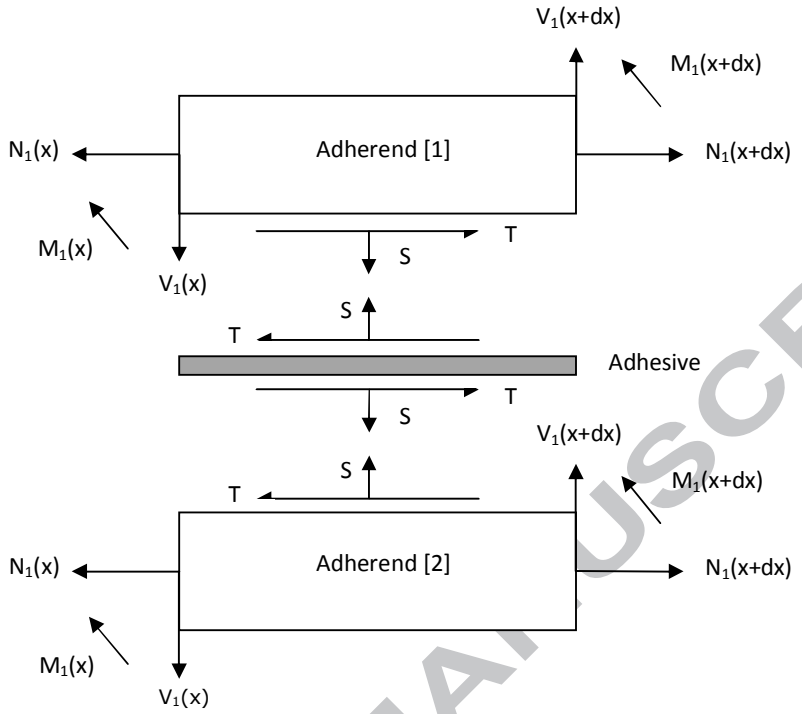


DCB specimen

Figure A3-8. Evolution of the adhesive peel and shear stresses at crack tip as a function of the number of elements within the length of the adhesive bondline. Convergence of the solution facing non-linear adhesive deformations. Convergence of the semi-analytical models.

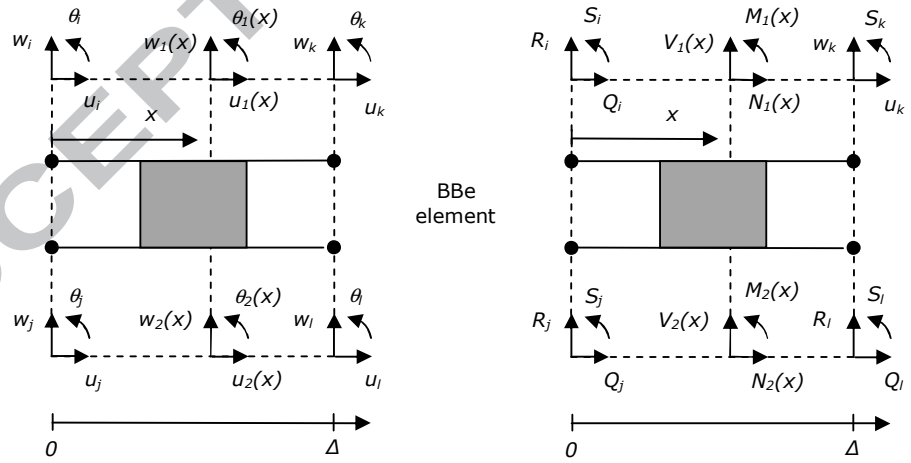
ACCEPTED MANUSCRIPT

Figures



N_j : Normal force of adherend (j) [N] ; V_j : Shear force of adherend (j) [N] ; M_j : Bending moment of adherend (j) [Nm] ; T : Adhesive shear stress [Mpa] ; S : Adhesive peel stress [Mpa] ;

Figure 1. Schematic representation of the local equilibrium of the bonded adherends. Linear elastic 1D-beam model.



u_j : normal displacement of adherend (j) [mm] ; w_j : transverse displacement of adherend (j) [mm] ; θ_j : bending angle of adherend (j) [rad] ; N_j : Normal force of adherend (j) [N] ; V_j : Shear force of adherend (j) ; M_j : Bending moment of adherend (j) [Nm] ;

Figure 2. Definition of the nodal displacements (forces) acting onto the BBe element. Linear elastic 1D-beam model.

ACCEPTED MANUSCRIPT

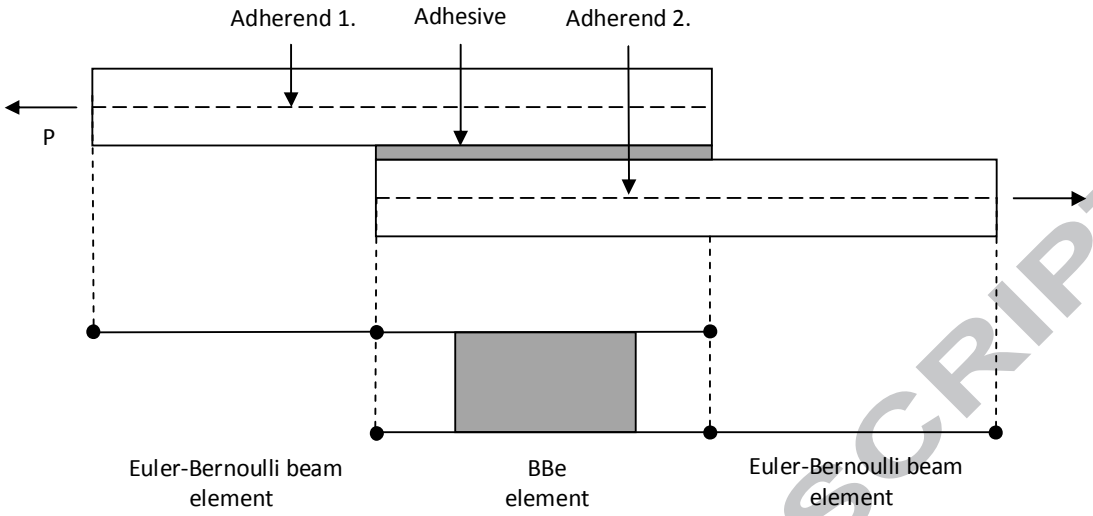
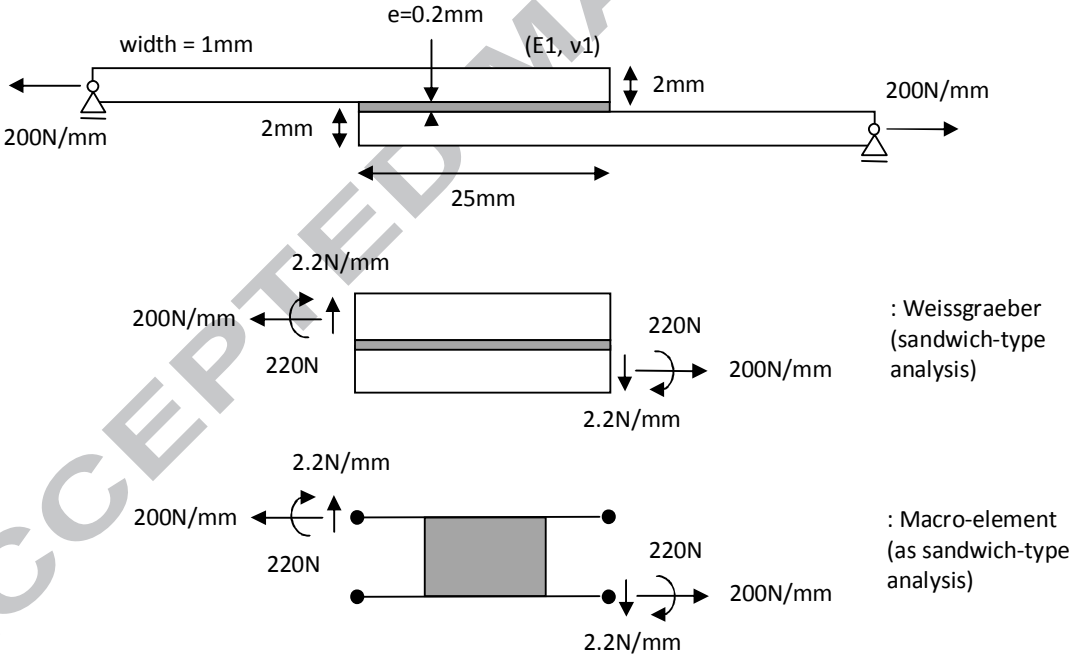


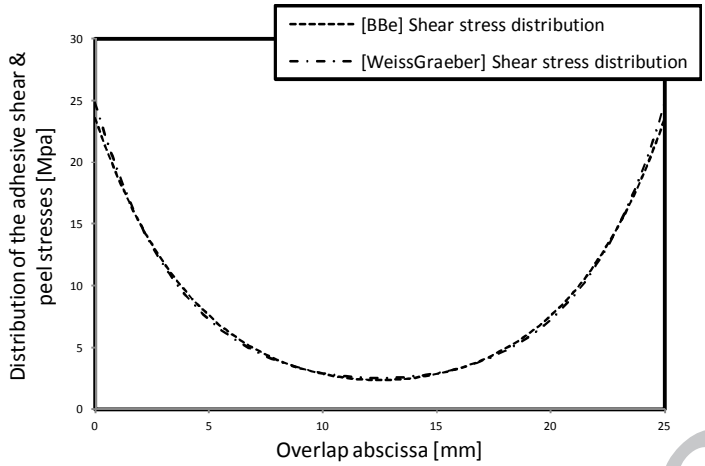
Figure 3. Assembly of the Single-Lap Joint (SLJ) configuration. Linear elastic 1D-beam model.



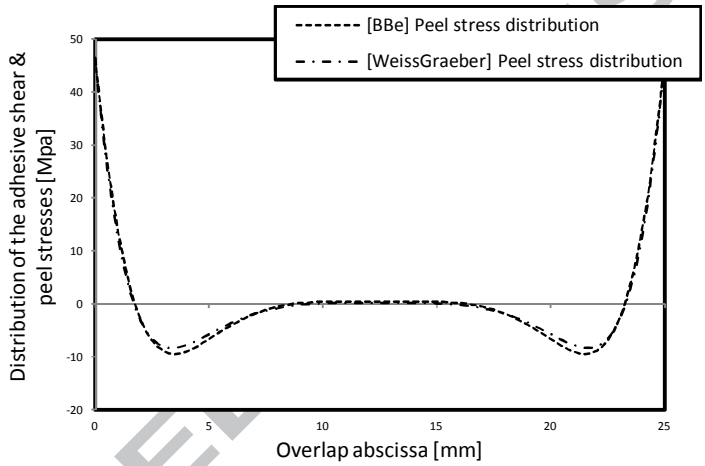
e_1: Thickness of the upper/lower adherend [mm] ; k_{GR}: Goland&Reissner's moment factor ; P: applied load [=2500N/10mm] ; E_1: Young's modulus of the upper/lower adherend [=210000 MPa] ; v_1: Poisson's ratio of the upper/lower adherend [=0.3] ; e: Thickness of the adhesive layer [mm] ; E: Peel modulus of the adhesive layer [=6554MPa] ; G: Shear modulus of the adhesive layer [=1433MPa] ;

Figure 4. Schematic representation of the Single-Lap Joint (SLJ) adhesive specimen. Loads acting onto the sandwich edges. Comparison with existing sandwich-type models.

ACCEPTED MANUSCRIPT

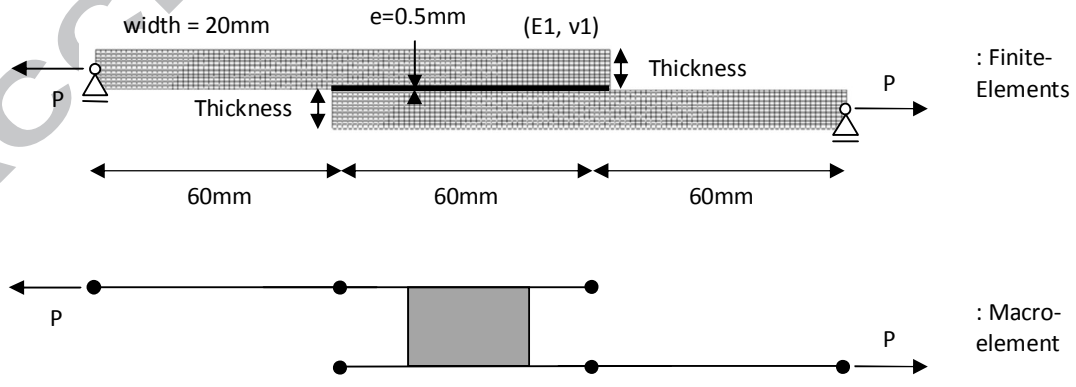


(a) Overlap shear stress distribution



(b) Overlap peel stress distribution

Figure 5. Comparison of the predicted adhesive shear and peel stress distributions along the overlap. Weissgraeber versus BBe. Single-Lap Joint (SLJ) configuration. Comparison with existing sandwich-type models.

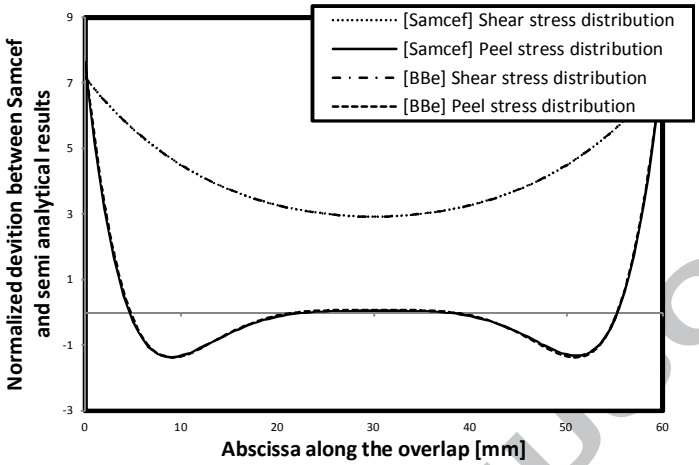


e_1: Thickness of the upper/lower adherend ; P: applied load [=5000N/20mm] ; E_1: Young's modulus of the upper/lower adherend [=72400 MPa] ; v_1: Poisson's ratio of the upper/lower adherend [=0.33] ; e: Thickness

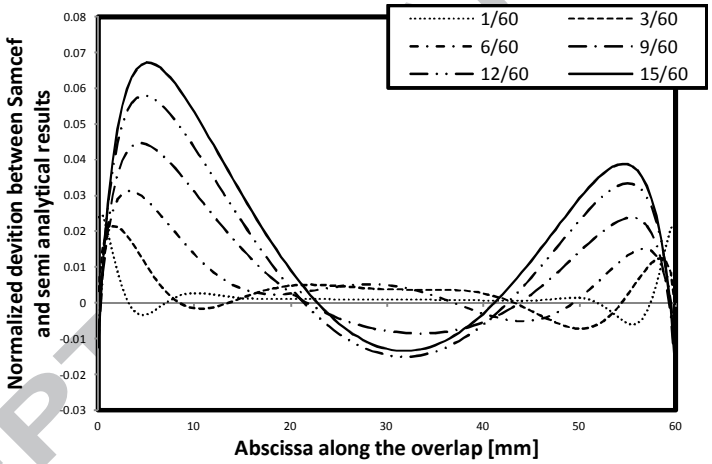
ACCEPTED MANUSCRIPT

of the adhesive layer [mm] ; E: Peel modulus of the adhesive layer [=185MPa] ; G: Shear modulus of the adhesive layer [=65MPa] ;

Figure 6. Schematic representation of the Single-Lap Joint (SLJ) adhesive specimen. Comparison with Finite Elements Analyses.

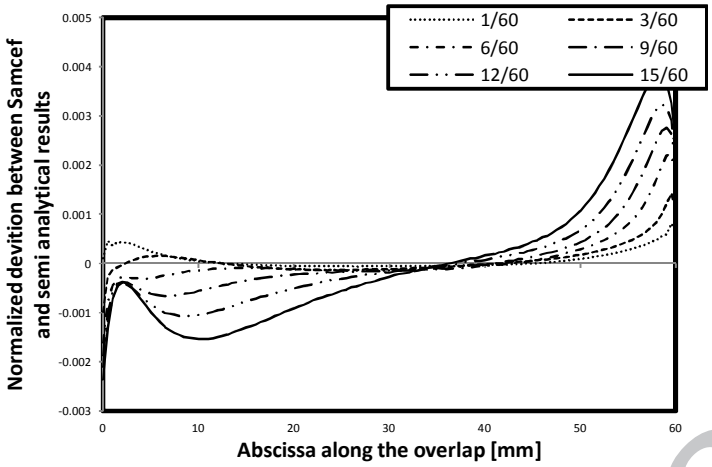


(b) Overlap peel and shear stress distributions. Adherends thickness =3mm.



(b) Normalized deviation between Finite Elements and semi-analytical peel stress distributions for various adherend thicknesses

ACCEPTED MANUSCRIPT



(c) Normalized deviation between Finite Elements and semi-analytical shear stress distributions for various adherend thicknesses

Figure 7. Comparison of the predicted adhesive shear and peel stress distributions along the overlap. Finite Element (FE) versus BBe. Single-Lap Joint configuration. Comparison with Finite Elements Analyses.

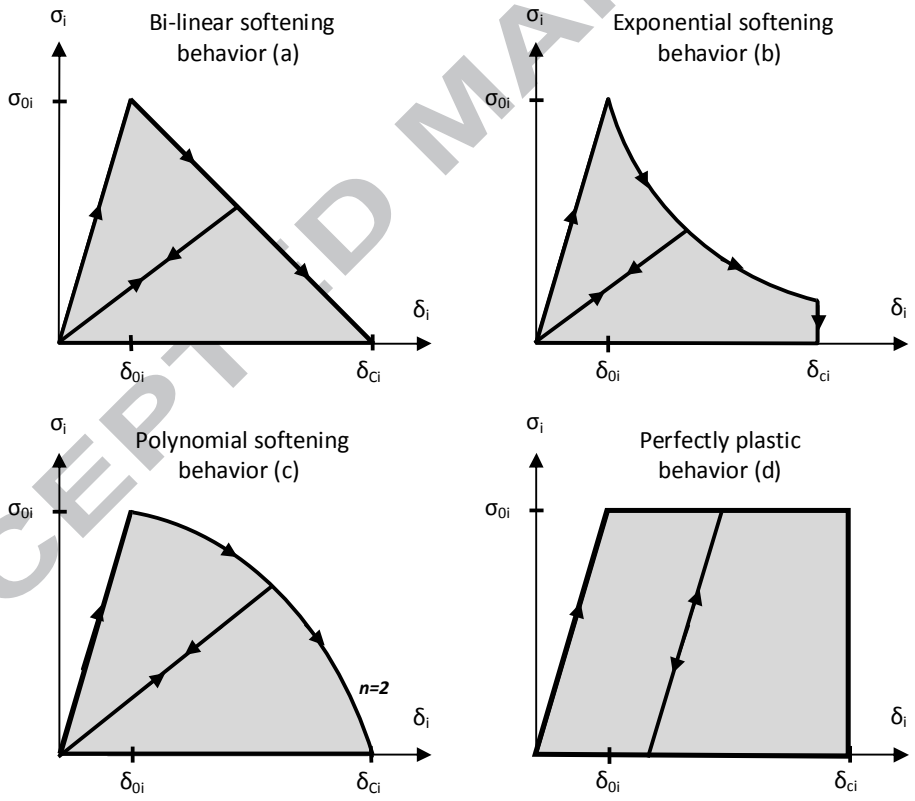


Figure 8. Restriction to bi-linear (a), exponential (b), polynomial (c) and perfectly plastic (d) softening behaviors. However the procedure is not limited to these particular behaviors only. Semi-analytical cohesive zone modeling.

ACCEPTED MANUSCRIPT

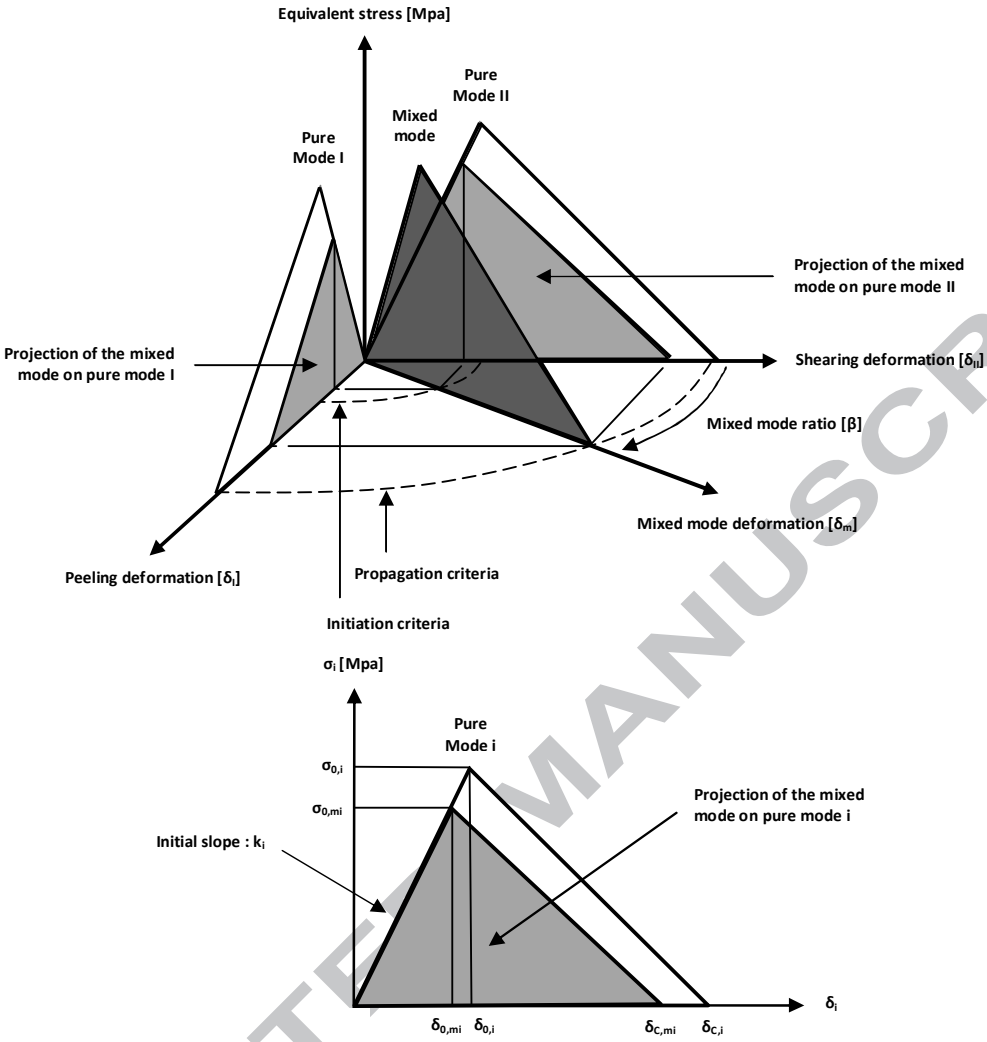


Figure 9. Graphical representation of the mixed-mode parameters. Description of the mixed-mode I/II adhesive behavior.

Tab 1. Examples of initiation/propagation mixed-mode criteria. Description of the pure mode adhesive behavior.

Linear energetic criterion (Reeder 1992)	Benzeggagh-Kenane criterion (Reeder 1992, Kenane 1997)
$\frac{G_{C,mI}}{G_{C,I}} + \frac{G_{C,mII}}{G_{C,II}} - 1 = 0$	$G_{C,I}\left(G_{C,II} - G_{C,I}\right)\left(\frac{G_{C,mII}}{G_{C,mI} + G_{C,mII}}\right)^{\eta} - \left(G_{C,mI} + G_{C,mII}\right) = 0$
Quadaratic energetic criterion (Reeder 1992)	JR Reeder criterion (Reeder 1992)
$\left(\frac{G_{C,mI}}{G_{C,I}}\right)^2 + \left(\frac{G_{C,mII}}{G_{C,II}}\right)^2 - 1 = 0$	$G_{C,I} + \rho\left(\frac{G_{0,mII}}{G_{0,II}}\right) + \upsilon\left(\frac{G_{0,mII}}{G_{0,II}}\right)^2 - \left(G_{C,mI} + G_{C,mII}\right) = 0$

ACCEPTED MANUSCRIPT

Tab 2. Mathematical representation of classical softening adhesive behaviors. Description of the pure mode adhesive behavior.

i=(I,II)	Linear elastic representation ($\delta_i<\delta_{0,i}$)	Non-linear softening representation ($\delta_{0,i}<\delta_i<\delta_{C,i}$)
Linear elastic	$\sigma_i(\delta_i) = k_i\delta_i$	N.A
Bi-linear cohesive damage	$\sigma_i(\delta_i) = k_i\delta_i$	$\sigma_i(\delta_i) = \left[1-\left(1-\frac{\delta_{0,i}(\delta_{C,i}-\delta_i)}{\delta_i(\delta_{C,i}-\delta_{0,i})}\right)\right]k_i\delta_i$
Polynomial cohesive damage	$\sigma_i(\delta_i) = k_i\delta_i$	$\sigma_i(\delta_i) = \left[1-\left(1-\frac{\delta_{0,i}(\delta_{c,i}^n-\delta_i^n)}{\delta_i(\delta_{c,i}^n-\delta_{0,i}^n)}\right)\right]k_i\delta_i$
Exponential cohesive damage	$\sigma_i(\delta_i) = k_i\delta_i$	$\sigma_i(\delta_i) = \left[1-\left(1-exp\left(1-\delta_i/\delta_{0,i}\right)\right)\right]k_i\delta_i$
Perfectly plastic cohesive law	$\sigma_i(\delta_i) = k_i\delta_i$	$\sigma_i(\delta_i) = \left[1-\left(1-\frac{\delta_{0,i}}{\delta_i}\right)\right]k_i\delta_i$

Tab 3. Mathematical description of the elastic energy ($Y_{0,i}$) and the fracture energy ($G_{C,i}$) of pure mode i (i=I,II). Description of the pure mode adhesive behavior.

i=(I,II)	Elastic Energy ($Y_{0,i}$)	Fracture Energy ($G_{C,i}$)
Linear elastic	$Y_{0,i} = \frac{1}{2}k_i\delta_{0,i}^2$	N.A
Bi-linear cohesive damage	$Y_{0,i} = \frac{1}{2}k_i\delta_{0,i}^2$	$G_{C,i} = Y_{0,i}\left[1+\left(\frac{\delta_{C,i}}{\delta_{0,i}}-1\right)\right] = \frac{1}{2}k_i\delta_{0,i}\delta_{C,i}$
Polynomial cohesive damage	$Y_{0,i} = \frac{1}{2}k_i\delta_{0,i}^2$	$G_{C,i} = Y_{0,i}\left[1+2\frac{\delta_{C,i}^n(\delta_{C,i}-\delta_{0,i})}{\delta_{0,i}(\delta_{C,i}^n-\delta_{0,i}^n)}\left(1-\frac{1}{n+1}\frac{(\delta_{C,i}^{n+1}-\delta_{0,i}^{n+1})}{\delta_{C,i}^n(\delta_{C,i}-\delta_{0,i})}\right)\right]$
Exponential cohesive damage	$Y_{0,i} = \frac{1}{2}k_i\delta_{0,i}^2$	$G_{C,i} = Y_{0,i}\left[5-2\left(\frac{\delta_{C,i}}{\delta_{0,i}}+1\right)exp\left(1-\frac{\delta_{C,i}}{\delta_{0,i}}\right)\right]$
Perfectly plastic cohesive law	$Y_{0,i} = \frac{1}{2}k_i\delta_{0,i}^2$	$G_{C,i} = Y_{0,i}\left[1+2\left(\frac{\delta_{C,i}}{\delta_{0,i}}-1\right)\right]$

ACCEPTED MANUSCRIPT

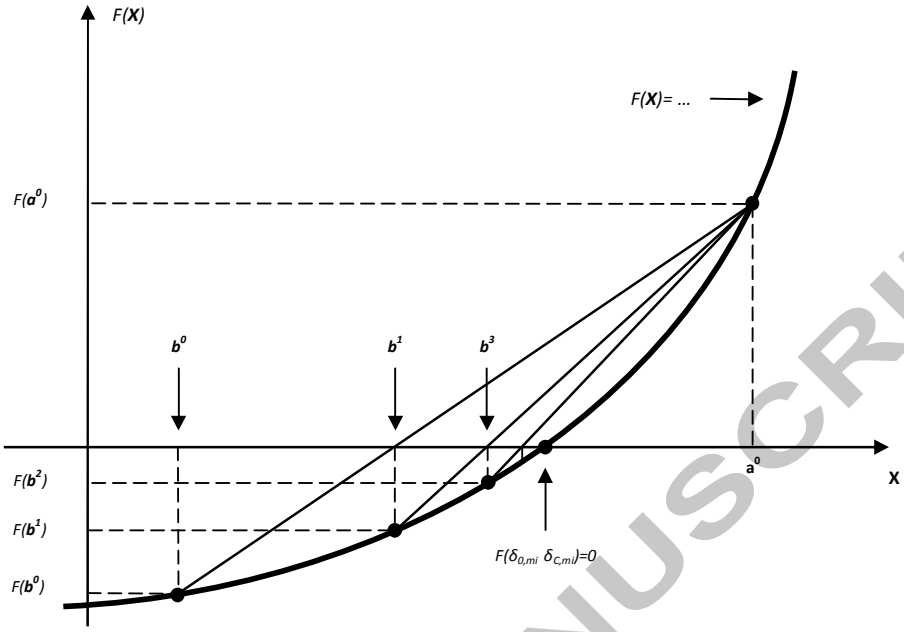


Figure 10. False position method. Computation of the effective initiation/propagation properties of the adhesive layer. Combination of the pure mode adhesive behaviors.

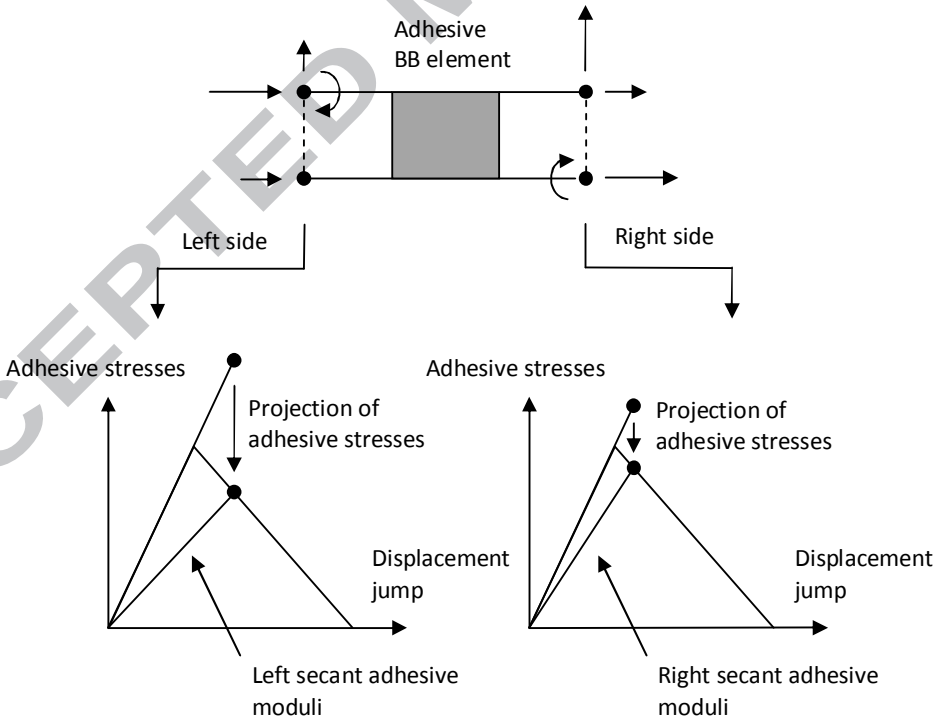


Figure 11. Dissimilar left side and right side adhesive secant stiffnesses. Computation of the secant stiffness matrix K_S. Adaptation of the Newton-Raphson procedure. Computation of the vector of imbalanced loads.

ACCEPTED MANUSCRIPT

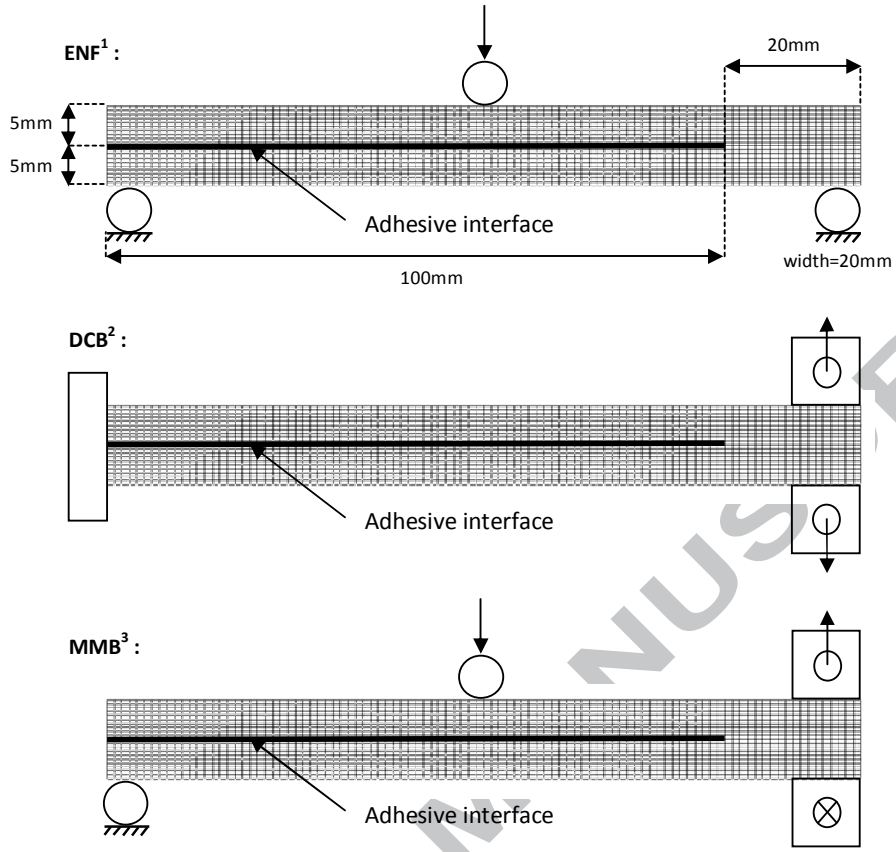


Figure 12. Schematic representation of the End-Notched Flexure (ENF), Double Cantilever Beam (DCB) and Mixed-Mode Bending (MMB) adhesive specimens. Description of the Finite Element (FE) models.

Tab 4. Adherend elastic properties. Description of the Finite Element (FE) models.

Adherends elastic properties.			
E	74200 Mpa	ν	0.34
G	27900 Mpa		-

Tab 5. Adhesive cohesive properties. Description of the Finite Element (FE) models.

Adhesive properties.			
k_I	185 Mpa	k_{II}	65 Mpa
$Y_{0,I}$	2. J/mm^2	$Y_{0,II}$	2. J/mm^2
$G_{C,I}$	4. J/mm^2	$G_{C,II}$	5. J/mm^2
Initiation criteria	Linear energetic	Propagation criteria	Linear energetic

ACCEPTED MANUSCRIPT

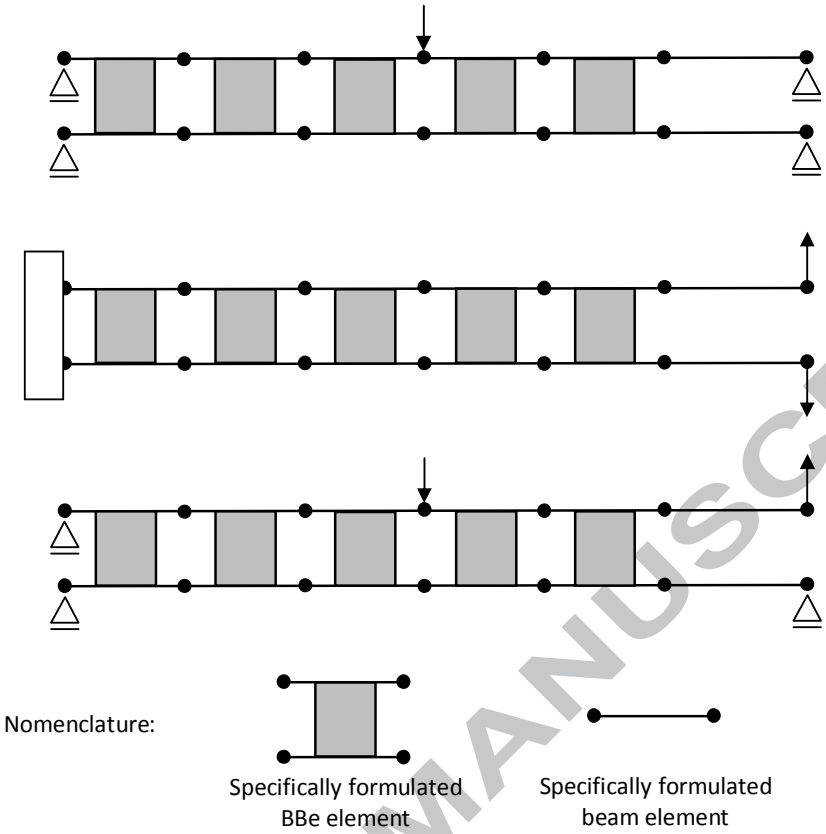
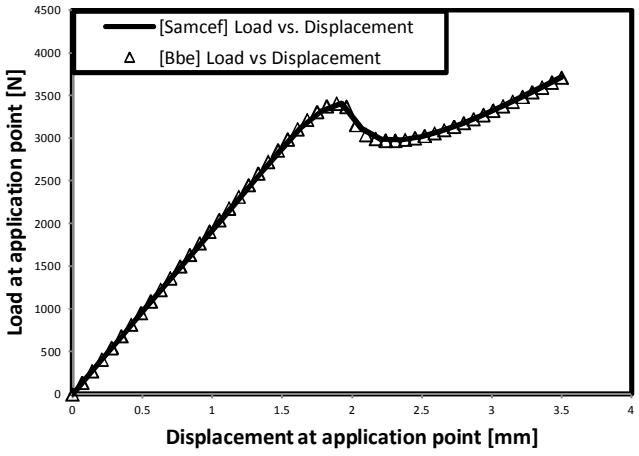
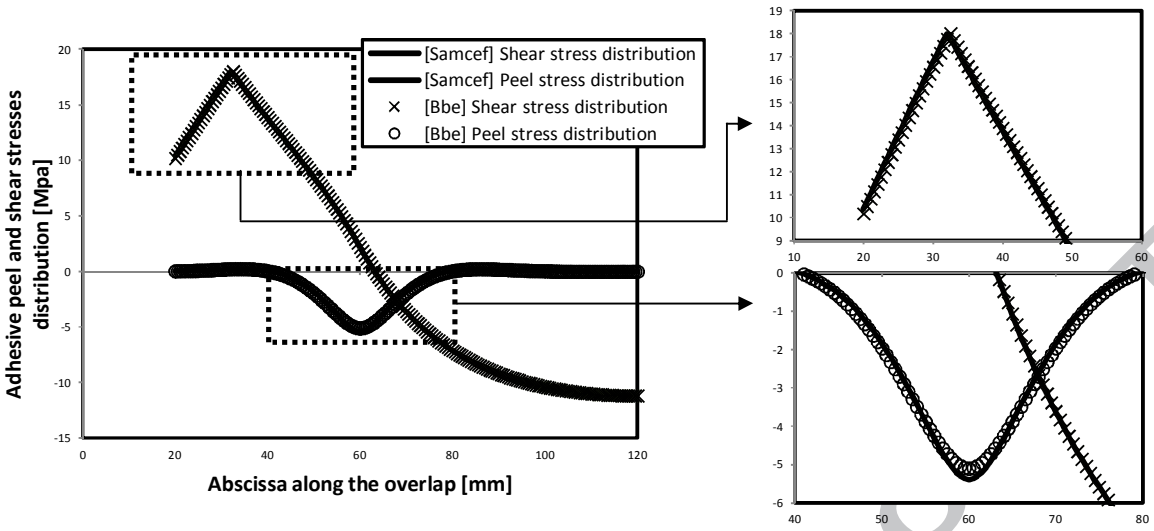


Figure 13. Schematic representation of End-Notched Flexure (ENF), Double Cantilever Beam (DCB) and Mixed-Mode Bending (MMB) adhesive specimens. Description of the semi-analytical models.

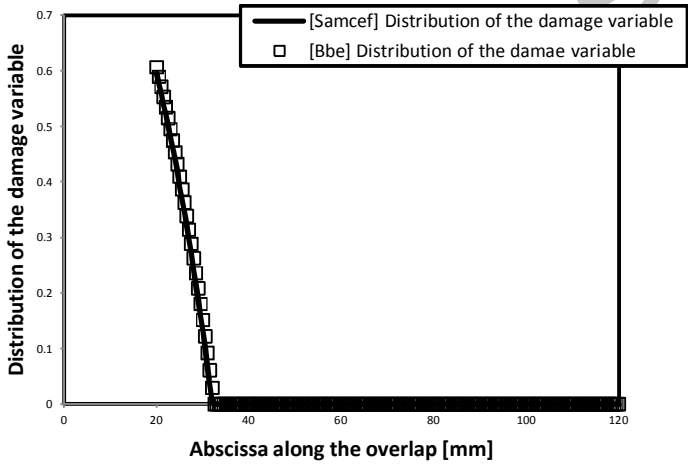


Load versus displacement (a)

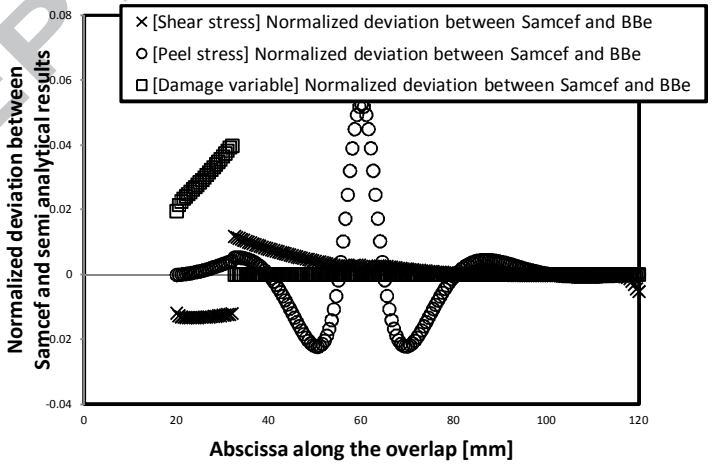
ACCEPTED MANUSCRIPT



Adhesive shear and stress distributions (b)



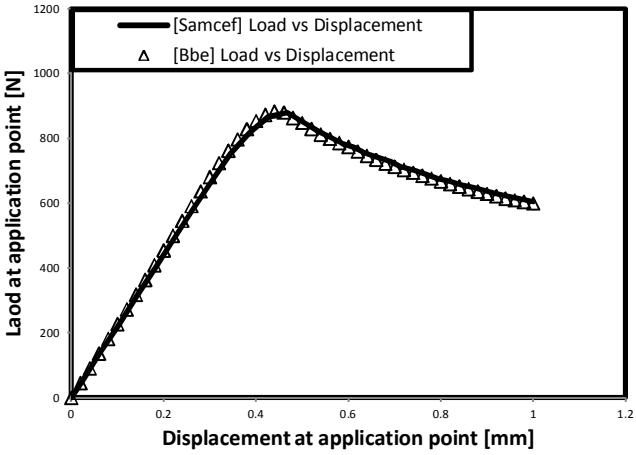
Distribution damage variable (c)



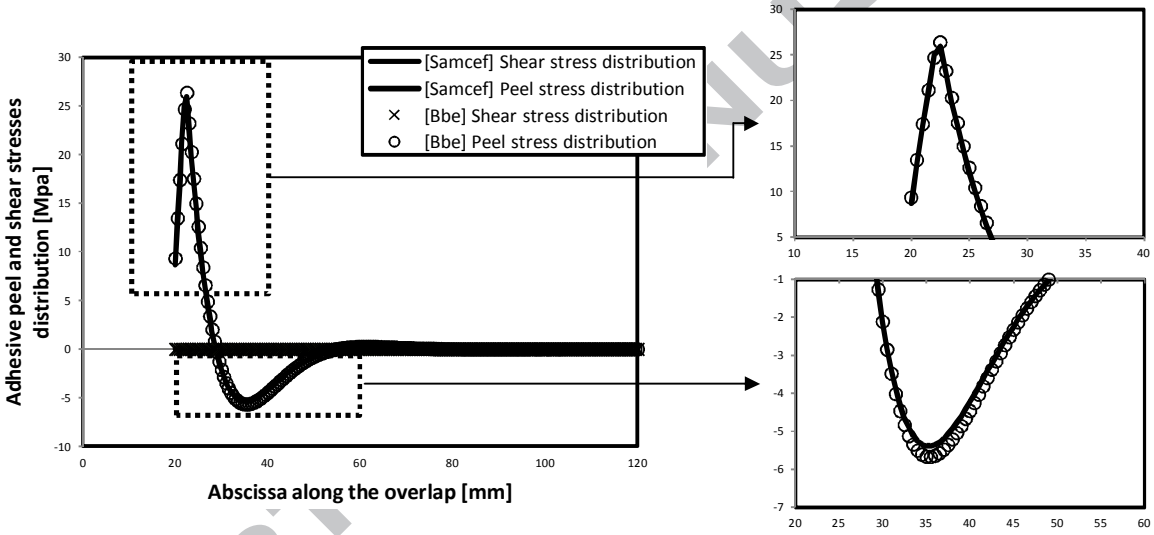
Absolute deviation between Samcef and semi-analytical results (d)

Figure 14. Comparison between semi-analytical results and Finite Element Analyses (FEA). End-Notched Flexure (ENF) specimen. Confrontation with classical Finite Element (FE) predictions.

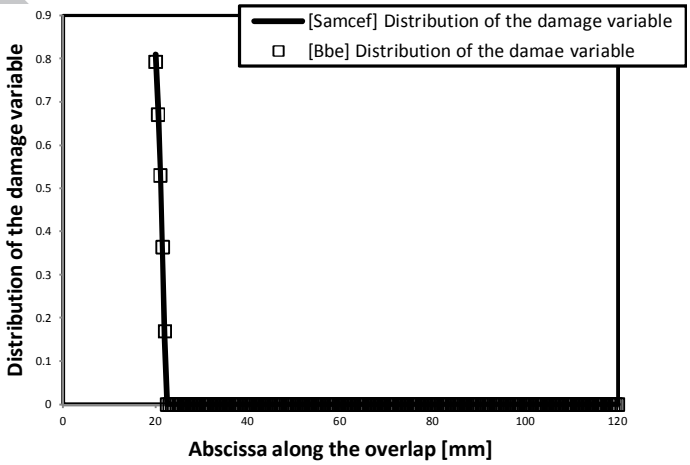
ACCEPTED MANUSCRIPT



Load versus displacement (a)

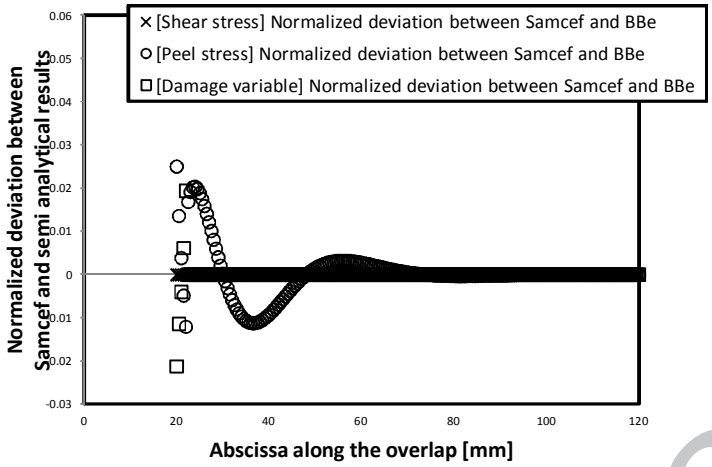


Adhesive shear and stress distributions (b)



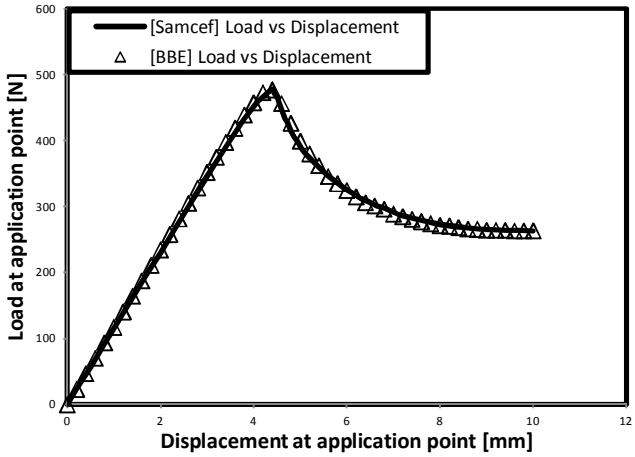
Distribution damage variable (c)

ACCEPTED MANUSCRIPT

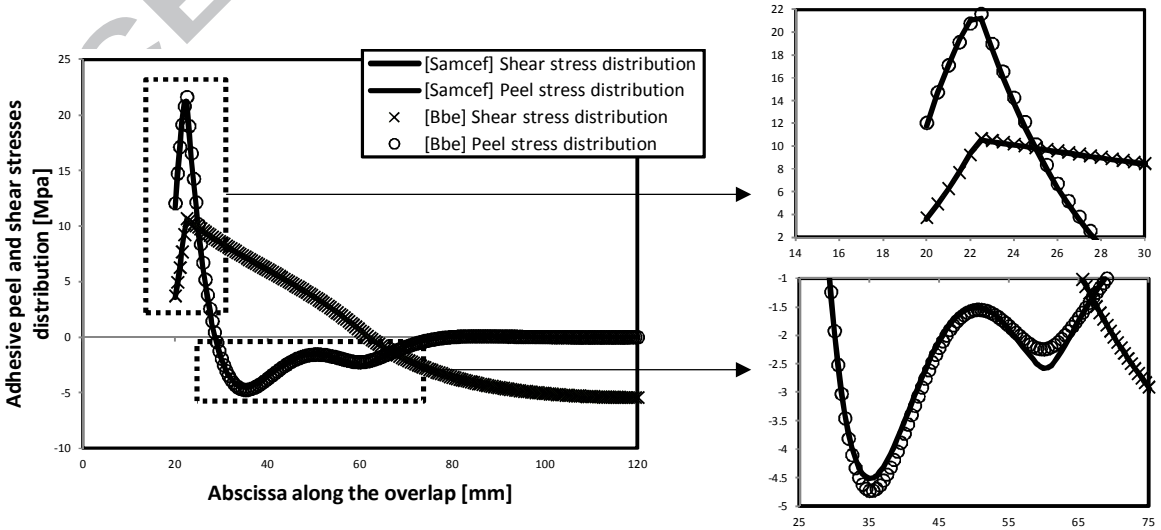


Absolute deviation between Samcef and semi-analytical results (d)

Figure 15. Comparison between semi-analytical results and Finite Element Analyses (FEA). Double Cantilever Beam (DCB) specimen. Confrontation with classical Finite Element (FE) predictions.

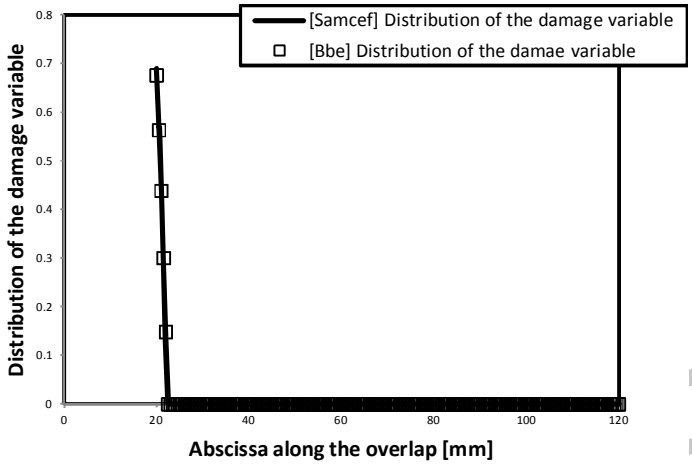


Load versus displacement (a)

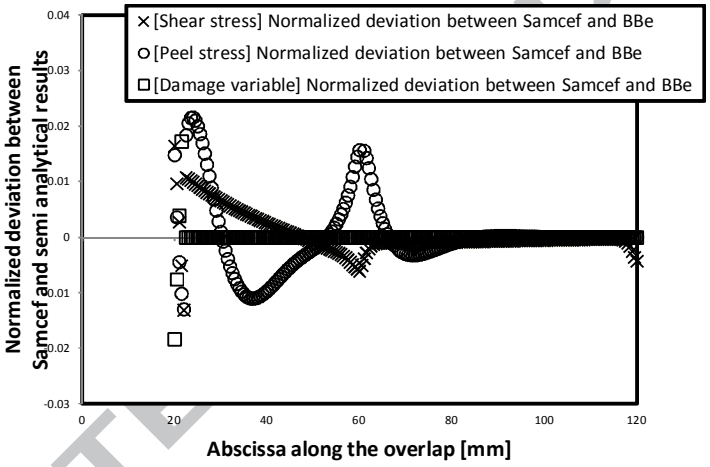


ACCEPTED MANUSCRIPT

Adhesive shear and stress distributions (b)



Distribution damage variable (c)



Absolute deviation between Samcef and semi-analytical results (d)

Figure 16. Comparison between semi-analytical results and Finite Element Analyses (FEA). Mixed-Mode Bending (MMB) specimen. Confrontation with classical Finite Element (FE) predictions.

ACCEPTED MANUSCRIPT

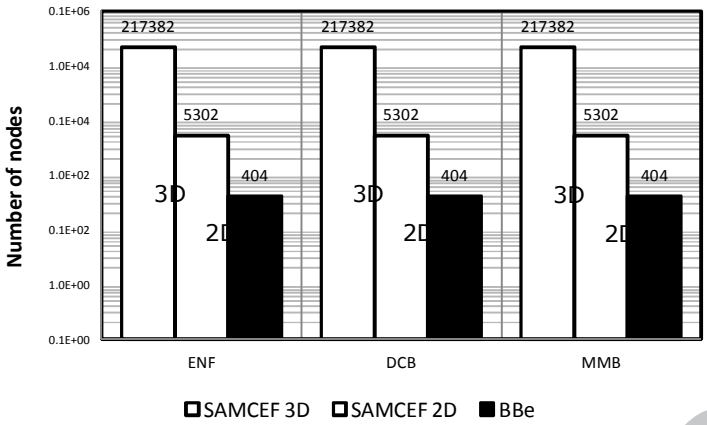


Figure 17. Comparison between semi-analytical and Finite Element (FE) predictions. Converged stress distributions. Comparison of the total number of degrees of freedom.

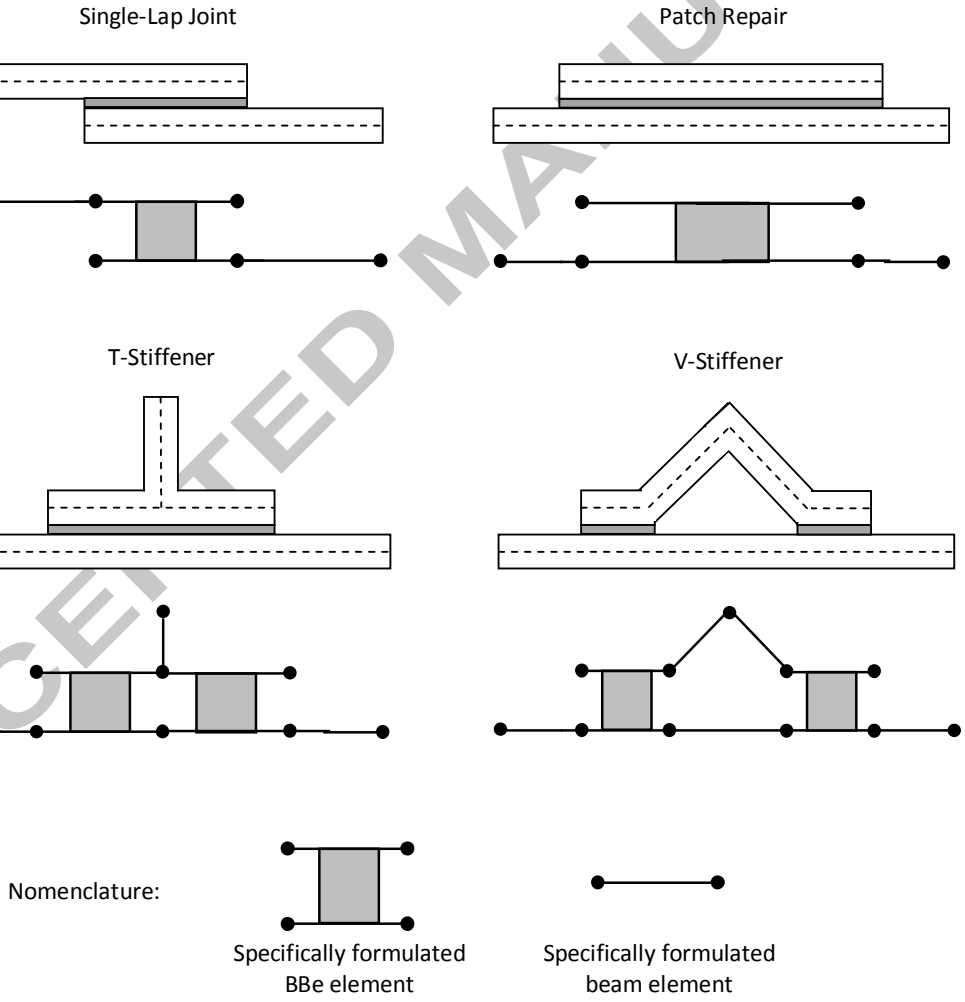


Figure 18. BBe elements as bricks of larger models for linear and non-linear adhesive stress analyses. Discussion.